

**PAPER****Ordering dynamics and aging in the symmetrical threshold model**David Abella¹ , Juan Carlos González-Avella^{1,2}, Maxi San Miguel¹ and José J Ramasco^{1,*}¹ Instituto de Física Interdisciplinar y Sistemas Complejos IFISC (CSIC—UIB), Campus Universitat Illes Balears, 07122 Palma de Mallorca, Spain² Advanced Programming Solutions SL, Palma de Mallorca, Spain

* Author to whom any correspondence should be addressed.

E-mail: jose.ramasco@csic.es**Keywords:** threshold model, complex contagion, ordering dynamics**OPEN ACCESS**RECEIVED
6 July 2023REVISED
14 December 2023ACCEPTED FOR PUBLICATION
4 January 2024PUBLISHED
17 January 2024Original Content from
this work may be used
under the terms of the
[Creative Commons
Attribution 4.0 licence](https://creativecommons.org/licenses/by/4.0/).Any further distribution
of this work must
maintain attribution to
the author(s) and the title
of the work, journal
citation and DOI.**Abstract**

The so-called Granovetter–Watts model was introduced to capture a situation in which the adoption of new ideas or technologies requires a certain redundancy in the social environment of each agent to take effect. This model has become a paradigm for complex contagion. Here we investigate a symmetric version of the model: agents may be in two states that can spread equally through the system via complex contagion. We find three possible phases: a mixed one (dynamically active disordered state), an ordered one, and a heterogeneous frozen phase. These phases exist for several configurations of the contact network. Then, we consider the effect of introducing aging as a non-Markovian mechanism in the model, where agents become increasingly resistant to change their state the longer they remain in it. We show that when aging is present, the mixed phase is replaced, for sparse networks, by a new phase with different dynamical properties. This new phase is characterized by an initial disordering stage followed by a slow ordering process toward a fully ordered absorbing state. In the ordered phase, aging modifies the dynamical properties. For random contact networks, we develop a theoretical description based on an approximate master equation that describes with good accuracy the results of numerical simulations for the model with and without aging.

1. Introduction

In recent decades, various techniques of probability and statistical physics have been employed to measure and explain social phenomena [1–3]. A variety of social collective phenomena can be well understood through stochastic binary-state models of interacting agents. In these models, each agent is assumed to be in one of two possible states, such as susceptible/infected, adopters/non-adopters, etc depending on the context of the model. The interaction among agents is determined by the underlying contact network and the dynamical rules of the model. There are various examples of binary-state models, including processes of opinion formation [4–8] and disease or social contagion [9, 10], among others. The consensus problem consists of determining under which circumstances the agents end up sharing the same state or when the coexistence of both states prevails. This is characterized by a phase diagram that provides the boundaries separating domains of different behaviors in the control parameter space. Macroscopic descriptions of these models in terms of mean-field, pair, and higher-order approximations are well established [11].

An important category of binary-state models are threshold models [12], which were originally introduced by Granovetter [9] to address problems of social contagion such as rumor propagation, innovation adoption, riot participation, etc. Multiple exposures, or group interaction, are necessary in these models to update the current state, a characteristic of complex contagion models [13, 14]. The threshold model presents a discontinuous phase transition from a ‘global cascade’ phase to a ‘no cascade’ phase, which was analyzed in detail in [12]. This model has been extensively studied on various network topologies, such as regular lattices, small-world [13], random [15], clustered [16, 17], modular [18], hypergraphs [19], homophilic [20] and coevolving [21] networks.

A main difference between the threshold model and other binary-state models, such as the Voter [4], majority vote [22–24], and nonlinear Voter model [25–30], is the lack of symmetry between the two states. In the threshold model, changing state is only possible in one direction, representing the adoption forever of a new state that initially starts in a small minority of agents. A symmetric version of the threshold model, with possible changes of states in both directions, was introduced in references [31, 32] to investigate the impact of noise and anticonformity. However, a complete characterization of the symmetrical threshold model and its ordering dynamics have not been addressed so far.

Aging is an important non-Markovian effect in binary-state models that has significant implications. It describes how the persistence time of an agent in a particular state influences the transition rate to a different state [33–37]. As such, the longer an agent remains in the current state, the smaller the probability of changing. Aging has been shown to cause coarsening dynamics toward a consensus state in the Voter model [34, 38], to induce bona fide continuous phase transitions in the noisy Voter model [39, 40], modify the phase diagram and non-equilibrium dynamics of the Schelling segregation model [41], and to modify non-trivially the cascade dynamics of the threshold model [42]. The introduction of aging is motivated by strong empirical evidence that human interactions do not occur at a constant rate and cannot be described using a Markovian assumption. Empirical studies have reported heavy-tail inter-event time distributions that reflect heterogeneous temporal activity patterns in social interactions [43–47].

In this work, we present a comprehensive analysis of the symmetrical threshold model, including its full phase diagram, and we investigate the effects of aging in the model. The model is examined in various network topologies, such as the complete graph, Erdős–Rényi (ER) [48], random regular (RR) [49], and a two-dimensional Moore lattice. The possible phases of the system are defined by the final stationary state as well as by the ordering/disordering dynamics characterized by the time-dependent magnetization, interface density, persistence, and mean internal time. For both the original model and the aging variant, the results of Monte Carlo (MC) numerical simulations are compared with results from the theoretical framework provided by an approximate master equation (AME) [42, 50] which is general for any random network. We also derive a mean-field analysis to describe the outcomes in a complete graph.

The article is organized as follows: in section 2, we describe the symmetrical threshold model and provide the numerical and theoretical analysis of the phase diagram. Each subsection reports the results for the different networks chosen. Section 3 presents the symmetrical threshold model with aging, the corresponding numerical and theoretical analysis, and the comparison with the model without aging. The results for the Moore lattice are shown in section 4. Finally, we conclude with a summary and conclusions in section 5.

2. Symmetrical threshold model

The system consists of a set of N agents located at the nodes of a network. The variable describing the state of each agent i takes one of the two possible values: $s_i = \pm 1$. Every agent has assigned a fixed threshold $0 \leq T \leq 1$, which determines the fraction of different neighbors required to change state. Even though this value might be agent-dependent, we will consider here only the case with a homogeneous T value for all the agents of the system. In each update attempt, an agent i (called active agent) is randomly selected, and if the fraction of neighbors with a different state is larger than the threshold T , the active agent changes state $s_i \rightarrow -s_i$. In other words, if m is the number of neighbors in state -1 out of the total number of neighbors k , the condition to change is $\theta(m/k - T)$, for a node in state $+1$, and $\theta((k - m)/k - T)$, for a node in state -1 , where $\theta(x)$ is the Heaviside step function. Notice that this update rule is equivalent to ‘shifted’ Glauber dynamics [51], with swapping probability $1/(1 + \exp[\beta(\Delta E + C)])$ (where β is the inverse temperature, ΔE the energy loss to swap the state of a node according to Ising Hamiltonian and C a shifting constant), at the limit of zero temperature ($\beta \rightarrow \infty$). We analyze the model dynamics using numerical simulations. Simulation time is measured in MC steps, i.e. N update attempts. Numerical simulations run until the system reaches a frozen configuration (absorbing state) or until the average magnetization, $m = (1/N) \sum_i s_i$, fluctuates around a constant value.

2.1. Mean-field

We first consider the mean-field case of the complete graph (all-to-all connections). We take an initial random configuration with magnetization m_0 and run numerical simulations for various values of T to construct the phase diagram (shown in figure 1(a)). We find three different phases based on the final state:

- **Phase I or mixed:** the system reaches an active disordered state (final magnetization $m_f = 0$) where the agents change their state continuously.
- **Phase II or ordered:** the system reaches the ordered absorbing states ($m_f = \pm 1$) according to the initial magnetization m_0 .

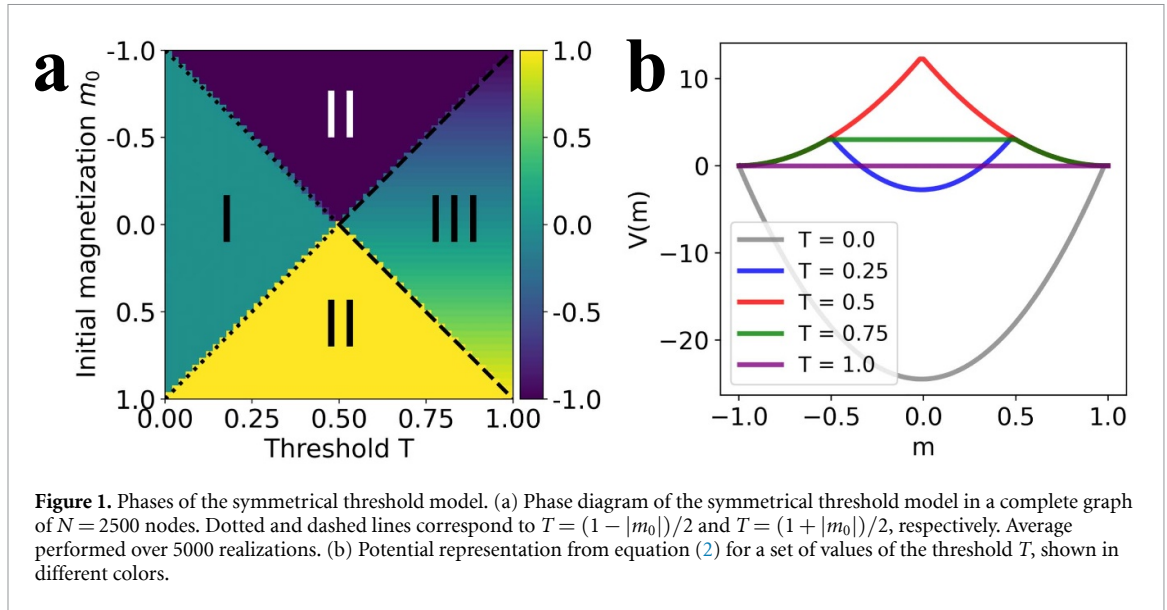


Figure 1. Phases of the symmetrical threshold model. (a) Phase diagram of the symmetrical threshold model in a complete graph of $N = 2500$ nodes. Dotted and dashed lines correspond to $T = (1 - |m_0|)/2$ and $T = (1 + |m_0|)/2$, respectively. Average performed over 5000 realizations. (b) Potential representation from equation (2) for a set of values of the threshold T , shown in different colors.

- **Phase III or frozen:** the system freezes at the initial random state $m_f = m_0$.

For a given initial magnetization $m_0 \neq 0$ and increasing T , the system undergoes a mixed-ordered transition at a critical threshold $T_c = (1 - |m_0|)/2$, and an ordered-frozen transition at a critical threshold $T_c^* = (1 + |m_0|)/2 > T_c$ (indicated by dotted and dashed black lines in figure 1(a), respectively). In this mean-field scheme, if the fraction of nodes in state $+1$ is denoted by x , the condition for a node in state -1 to change its state is given by $\theta(x - T)$, where θ is the Heaviside step function. Thus, in the thermodynamic limit ($N \rightarrow \infty$), the variable x evolves over time according to the following mean-field equation:

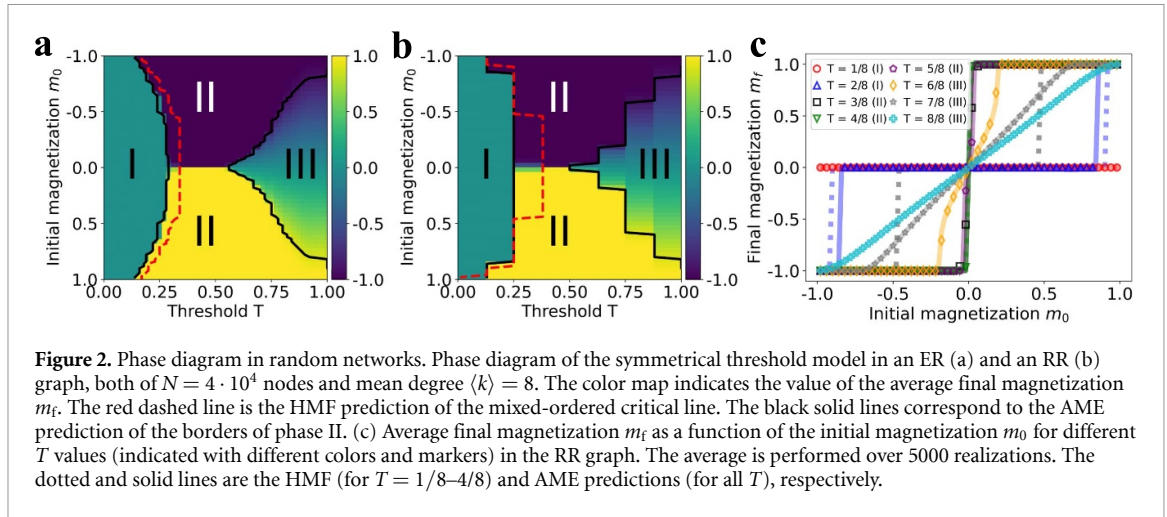
$$\frac{dx}{dt} = (1 - x) \theta(x - T) - x \theta(1 - x - T) = -\frac{\partial V(x)}{\partial x}. \quad (1)$$

Here, $V(x)$ is the potential function. The stationary value of x , x_{st} , is the solution of the implicit equation resulting from setting the time derivative equal to 0. The stationary solutions are $x_{st} = 1/2$ ($m = 0$), the absorbing states $x_{st} = 0, 1$ ($m = \pm 1$) or a degenerate continuum of solutions. The stability of these solutions can be understood in terms of the potential $V(x)$:

$$\begin{aligned} V(x) &= -\int (1 - x) \theta(x - T) - x \theta(1 - x - T) dx \\ &= \frac{x^2}{2} + \frac{1}{2} (T^2 - 2T - x^2 + 1) \theta(T + x - 1) \\ &\quad - \frac{1}{2} (T^2 - 2T - x(x - 2)) \theta(x - T). \end{aligned} \quad (2)$$

The minimum and maximum values of $V(x)$ correspond to stable and unstable solutions, respectively. Figure 1(b) shows the potential's dependence on the magnetization, obtained after a variable change $m = 2x - 1$ in equation (2). For $T < 0.5$, $m = 0$ is a stable solution, but increasing the threshold reduces the range of values of the initial magnetization from which this solution is reached, enclosing phase I between the unstable solutions $m = 1 - 2T$ and $2T - 1$. In fact, if $m_0 > 1 - 2T$, the system reaches the absorbing solution $m = +1$, while if $m_0 < -1 + 2T$, it reaches $m = -1$ (phase II). For $T = 0.5$, there is just one unstable solution at $m = 0$, and all the initial magnetization values reach the absorbing states $m = \pm 1$. For $T > 0.5$, the potential is equal to a constant value for a range of m_0 , which means that an initial condition will remain in this state forever (phase III). The range of values of the initial condition from which this phase is reached grows linearly with T until $T = 1$, where all initial conditions fulfill $\frac{dm}{dt} = 0$.

Note that the mean-field symmetrical threshold model for $T = 1$ shows the same potential profile as the mean-field Voter model [1, 4, 6]. The important difference is that for the Voter model, any initial magnetization is marginally stable, while in our model any initial magnetization is an absorbing state in phase III. In the Voter model finite size fluctuations will take the system to the absorbing states $m = \pm 1$.



2.2. Random networks

We analyze the phase diagram of the symmetrical threshold model in two random networks: ER [48] and RR [49] graphs with mean degree $\langle k \rangle = 8$. Figures 2(a) and (b) show the phase diagram for both networks, where it is shown that the existence of the three phases previously described is robust to changes in network structure. The main difference from the all-to-all scenario is that phase III does not freeze exactly at the same initial magnetization. Instead, the system reaches an absorbing state with a higher magnetization $m_f > m_0$. In this phase, the value of m_f depends on the threshold such that increasing T , increases the disorder in the system, until $T = 1$, where $m_f = m_0$ (see figure 2(c)). On the other hand, phases I and II reach the same stationary state as in the mean-field case. Furthermore, the critical thresholds T_c and T_c^* show a different dependence on m_0 depending on the network structure.

To explain the transitions exhibited by the model, we use a theoretical framework for binary-state dynamics in complex networks [50]: the AME, which considers agents in both states ± 1 with degree k , m neighbors in state -1 that have been j time steps in the current state (called ‘internal time’ or ‘age’) as different sets in a compartmental model (see details of the AME derivation in [42, 50]). In general, the AME is:

$$\begin{aligned} \frac{d}{dt} x_{k,m,0}^{\pm}(t) &= -x_{k,m,0}^{\pm}(t) + \sum_l T_{k,m,l}^{\mp} x_{k,m,l}^{\mp}(t) - (k-m) \beta^{\pm} x_{k,m,0}^{\pm}(t) - m \gamma^{\pm} x_{k,m,0}^{\pm}(t), \\ \frac{d}{dt} x_{k,m,j}^{\pm}(t) &= -x_{k,m,j}^{\pm}(t) + A_{k,m,j}^{\pm} x_{k,m,j-1}^{\pm}(t) - (k-m) \beta^{\pm} x_{k,m,j}^{\pm}(t) \\ &\quad + (k-m+1) \beta^{\pm} x_{k,m-1,j-1}^{\pm}(t) + (m+1) \gamma^{\pm} x_{k,m+1,j-1}^{\pm}(t) - m \gamma^{\pm} x_{k,m,j}^{\pm}(t), \end{aligned} \quad (3)$$

where variables $x_{k,m,j}^+(t)$ and $x_{k,m,j}^-(t)$ are the fractions of k -degree nodes that are in state $+1$ (respectively, -1) that have m neighbors in state -1 and age j . The configuration-dependent rates β^{\pm} account for the change of state of neighbors (\pm) of a node in state $+1$. The rates γ^{\pm} are equivalent but for nodes in state -1 . To build the AME, we need to assume that these rates are equal for all nodes in the same state, as in [50]:

$$\begin{aligned} \beta^+ &= \frac{\sum_j \sum_k p_k \sum_{m=0}^k (k-m) T_{k,m,j}^+ x_{k,m,j}^+}{\sum_j \sum_k p_k \sum_{m=0}^k (k-m) x_{k,m,j}^+}, \\ \beta^- &= \frac{\sum_j \sum_k p_k \sum_{m=0}^k m T_{k,m,j}^+ x_{k,m,j}^+}{\sum_j \sum_k p_k \sum_{m=0}^k m x_{k,m,j}^+}, \\ \gamma^+ &= \frac{\sum_j \sum_k p_k \sum_{m=0}^k (k-m) T_{k,m,j}^- x_{k,m,j}^-}{\sum_j \sum_k p_k \sum_{m=0}^k (k-m) x_{k,m,j}^-}, \\ \gamma^- &= \frac{\sum_j \sum_k p_k \sum_{m=0}^k m T_{k,m,j}^- x_{k,m,j}^-}{\sum_j \sum_k p_k \sum_{m=0}^k m x_{k,m,j}^-}, \end{aligned} \quad (4)$$

where the degree distribution of the chosen network is p_k . Notice that these equations are written using a dimensionless time t . The transition rate $T_{k,m,j}^{\pm}$ is for the probability of changing state ($\pm \rightarrow \mp$) for an agent

of degree k , m neighbors in state -1 and age j , while the aging rate $A_{k,m,j}^{\pm}$ is for the probability of staying in the same state and increasing the internal time ($j \rightarrow j + 1$). For the symmetrical threshold model, according to the update rules these rates do not depend on internal time j (Markovian dynamics):

$$\begin{aligned} T_{k,m,j}^+ &= \theta(m/k - T) & T_{k,m,j}^- &= \theta((k-m)/k - T), \\ A_{k,m,j}^{\pm} &= 1 - T_{k,m,j}^{\pm}. \end{aligned} \quad (5)$$

Therefore, if we were not concerned with the internal time dynamics, we can simplify our AME to the one proposed by Gleeson in [50] for general binary-state models. Here we keep the internal times for a dynamical characterization of the different phases and as a reference frame for the aging studies in the next section.

The AME is based in the same basic assumptions used in [50]: an uncorrelated network with negligible levels of clustering created using the configuration model [52] (using a degree distribution p_k). The approximation also neglects finite size effects, being only valid in the thermodynamic limit ($N \rightarrow \infty$). Notice that we cannot use the AME to describe the complete graph. For the complex networks considered in this section, these conditions are satisfied for large N , and the differential equations can be solved numerically using standard methods (a general script in Julia is available in the author's GitHub repository [53]). The mixed order and ordered frozen transitions predicted (solid black lines in figures 2(a) and (b), respectively) are in agreement with the numerical simulations. The predicted lines represent the initial and final values of T at which the AME reaches the ordered absorbing states $m_f = \pm 1$. In figure 2(c), we also observe a good agreement between numerically integrated solutions (solid colored lines) and numerical simulations (markers), which is quantified via the relative difference Δ (see at figure captions).

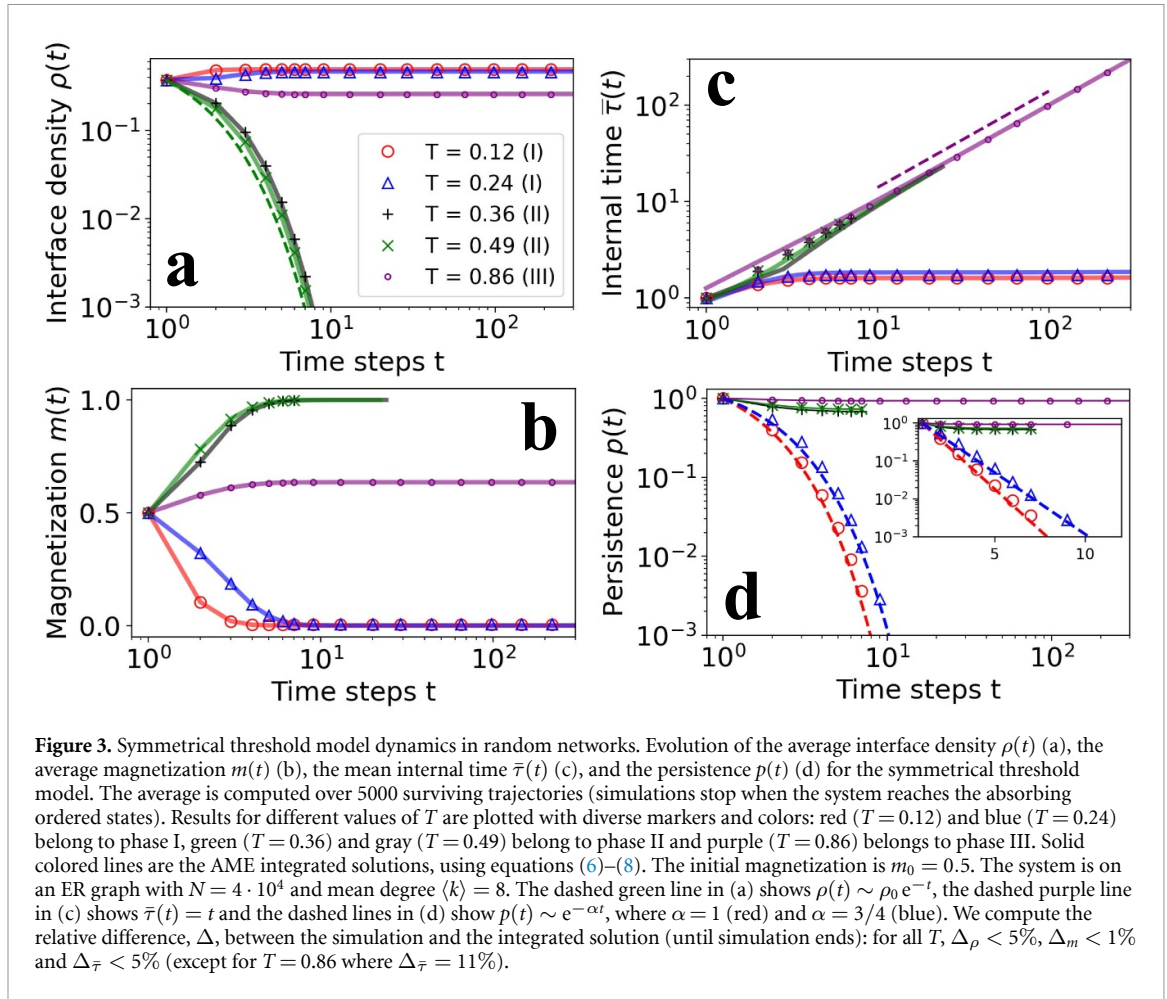
An alternative simpler approximation is to consider a heterogeneous mean-field (HMF) approximation (refer to appendix A for further details). This approximation is very useful when we work with networks with high clustering, close to the complete graph scenario ($\langle k \rangle / N \rightarrow 1$), a regime where the AME does not work properly because the clustering is not negligible. For our networks, HMF captures the qualitative behavior but the numerically integrated solutions do not agree with numerical simulations (see red dashed lines in figures 2(a) and (b)), and the colored dotted lines in figure 2(c), and the frozen phase is not predicted by this framework. These findings demonstrate that threshold models (in networks far from $\langle k \rangle / N = 1$) need approximations beyond mean-field to achieve accuracy, in agreement with the findings in [15, 42, 50].

Beyond the stationary states, the previous phases can be characterized by their ordering dynamical regimes. To describe the coarsening process, we use the time-dependent average interface density $\rho(t)$ (fraction of links between nodes in different states), the average magnetization $m(t)$, the mean internal time $\bar{\tau}(t)$ (mean time spent in the current state over all the nodes) and the persistence $p(t)$ (fraction of nodes that remain in their initial state at time t) [54]. Figure 3 shows the average results obtained from the numerical simulations, starting from an initial magnetization $m_0 = 0.5$. There are three regimes with different dynamical properties:

- **Mixed regime (phase I):** it corresponds to phase I in the static phase diagram and it is characterized by fast disordering dynamics, which is reflected by an exponential decay of the persistence. The interface density, the magnetization, and the mean internal time exhibit fast dynamics toward their asymptotic values in the dynamically active stationary state (see $T = 0.12, 0.24$ in figure 3).
- **Ordered regime (phase II):** it coincides with phase II in the static diagram and it is characterized by an exponential decay of the interface density. The magnetization tends to the ordered absorbing state based on the initial majority, and the mean internal time tends to scale as $\bar{\tau}(t) \sim t$. Persistence in this phase decays until a plateau that corresponds to the initial majority that reaches consensus (since this fraction of nodes does not change state from the initial condition). When consensus is reached, the surviving trajectory is stopped (see $T = 0.36, 0.49$ in figure 3).
- **Frozen regime (phase III):** this regime corresponds to phase III and it is characterized by an initial ordering process followed by the stop of the dynamics, with constant values of the metrics. The only exceptions are the mean internal time that grows as $\bar{\tau}(t) \sim t$ (see $T = 0.86$ in figure 3) and the persistence.

Using the numerically integrated solutions of AME ($x_{k,m,j}^{\pm}(t)$), we can compute the magnetization $m(t)$, the interface density $\rho(t)$, and the mean internal time $\bar{\tau}$:

$$\rho(t) = \frac{\sum_j \sum_k p_k \sum_m m x_{k,m,j}^+}{\frac{1}{2} \sum_j \sum_k p_k \sum_m k (x_{k,m,j}^+ + x_{k,m,j}^-)}, \quad (6)$$



$$\begin{aligned}
 m(t) &= 2 \sum_j \sum_k p_k \sum_m x_{k,m,j}^+ - 1 \\
 &= -2 \sum_j \sum_k p_k \sum_m x_{k,m,j}^-,
 \end{aligned} \tag{7}$$

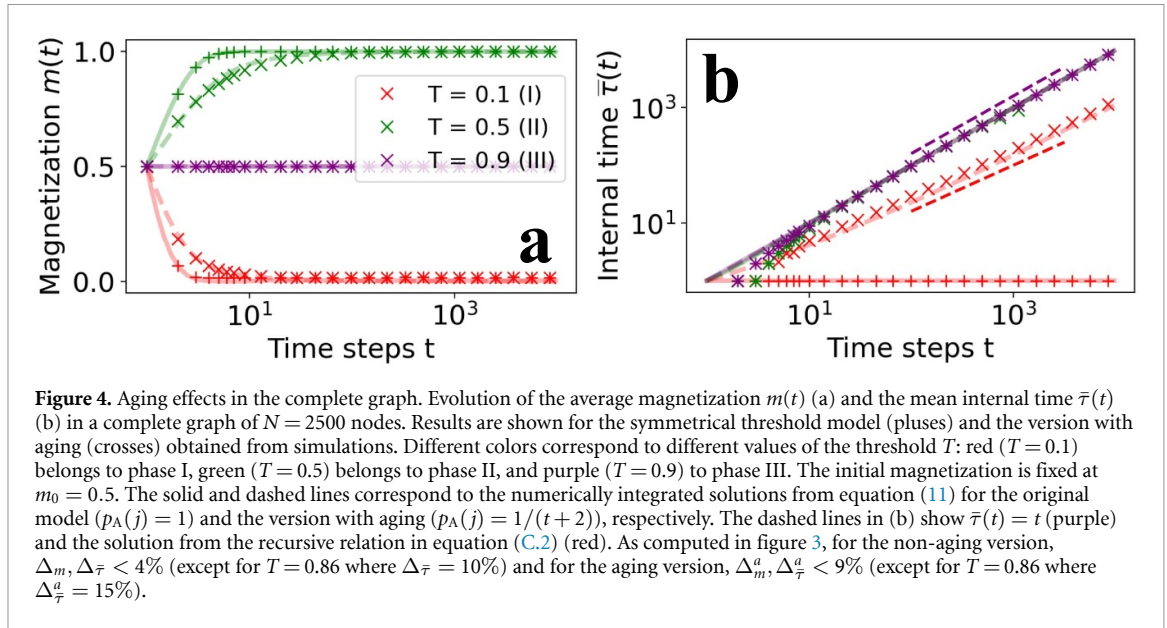
$$\bar{\tau}(t) = \sum_j \sum_k p_k \sum_m j \left(x_{k,m,j}^+ + x_{k,m,j}^- \right). \tag{8}$$

All metrics exhibit a strong agreement between the numerical simulations and the integrated solutions (see solid lines in figure 3). However, the persistence cannot be directly calculated from the integrated solutions. This is because the fraction of persistent nodes at time t corresponds to the fraction of nodes with internal time $j = t$, which is at an extreme of the age distribution at each time step, since $x_{k,m,j}^\pm(t) = 0$ for $j > t$. Therefore, the computation of this measure requires a more sophisticated analysis using extreme value theory [55].

We note that the dynamical characterization discussed above holds for all possible m_0 except for the symmetric initial condition $m_0 = 0$. In this case, an order–disorder transition arises at a critical mean degree k_c , whose value depends on the size of the system N [56].

3. Symmetrical threshold model with aging

Aging refers to the property of agents becoming less likely to change their state the longer they have remained in that state [33, 37–42, 46]. In contrast to the original model, which assumes that agents update their state at a constant rate, this model introduces an activation function $p_A(j)$ that is inversely proportional to the agent’s internal time j . At each time step, the following two steps are performed:



- (i) A node i with age j is selected at random and activated with probability $p_A(j)$.
- (ii) If the fraction of neighbors in a different state is greater than the threshold T , the activated node changes its state from s_i to $-s_i$ and resets its internal time to $j = 0$.

Following previous literature on aging effects [30, 34, 39, 41, 42] we make the choice of $p_A(j) = 1/(j+2)$ for the aging probability. This particular choice is motivated by the fact that it allows to reproduce inter-event time distributions observed empirically [44, 46].

3.1. Mean-field

Figure 4 compares the evolution of the average magnetization and mean internal time on a complete graph of the original symmetrical threshold model and the version with aging in phases I, II, and III. We observe that, for all considered threshold values, aging introduces a delay. However, the final stationary state coincides with the one observed for the original model. To explain these dynamics, we use an HMF approach that considers the effects of aging, as in [37] for other binary-state models (we use a general HMF description to be applied for a complete graph and to random networks in next section). In this case, the AME does not work well due to the high density of the network. For a general network with degree distribution p_k , we define the fraction of agents in state ± 1 with k neighbors and age j at time t as $x_{k,j}^{\pm}(t)$. The probability of finding a neighbor in state ± 1 is \tilde{x}^{\pm} , which can be written as

$$\tilde{x}^{\pm} = \sum_k p_k \frac{k}{\langle k \rangle} \sum_{j=0}^{\infty} x_{k,j}^{\pm}, \quad (9)$$

where $\langle k \rangle$ is the mean degree of the network. The transition rate $\omega_{k,j}^{\pm}$ for a node with state ± 1 , degree k and age j to change state is given by

$$\omega_{k,j}^{\pm} = p_A(j) \sum_{m=0}^k \theta\left(\frac{m}{k} - T\right) B_{k,m}[\tilde{x}^{\mp}], \quad (10)$$

where $B_{k,m}[x]$ is the binomial distribution with k attempts, m successes, and with the probability of success x . In our model, there are two possible events for a node with degree k and age j :

- It changes state and the age is reset to $j = 0$.
- It remains at its state and the age increases by one time step $j = j + 1$.

According to these possible events, we can write the rate equations for the variables $x_{k,j}^{\pm}$ and $x_{k,0}^{\pm}$ as

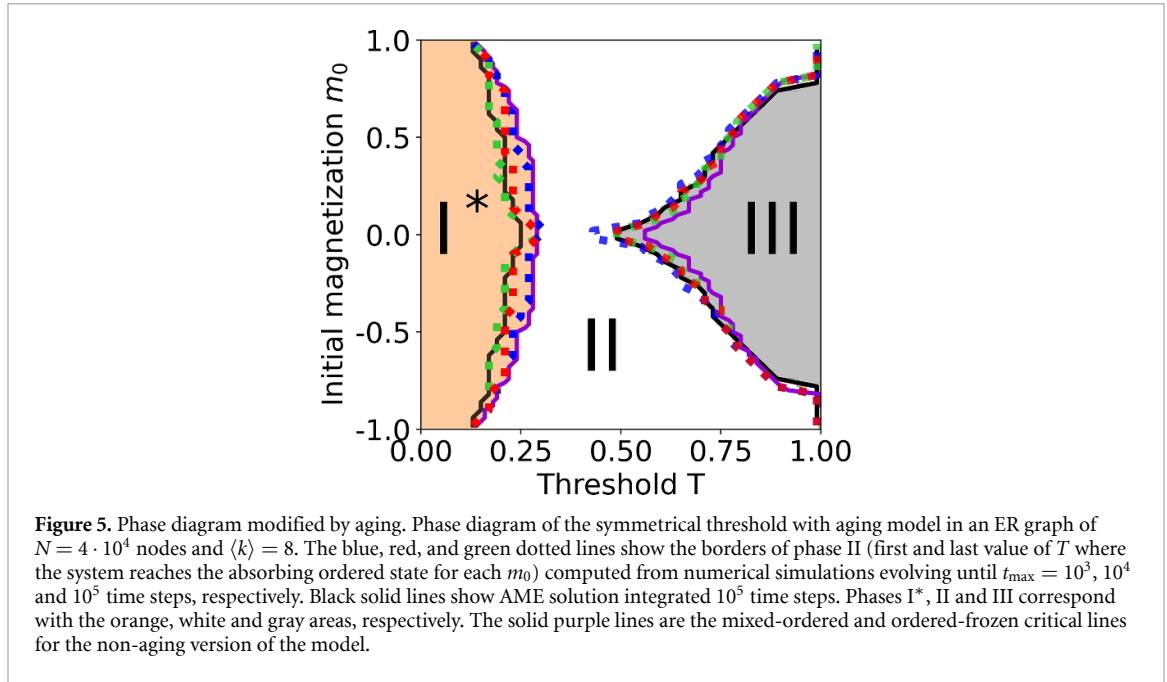


Figure 5. Phase diagram modified by aging. Phase diagram of the symmetrical threshold with aging model in an ER graph of $N = 4 \cdot 10^4$ nodes and $\langle k \rangle = 8$. The blue, red, and green dotted lines show the borders of phase II (first and last value of T where the system reaches the absorbing ordered state for each m_0) computed from numerical simulations evolving until $t_{\max} = 10^3, 10^4$ and 10^5 time steps, respectively. Black solid lines show AME solution integrated 10^5 time steps. Phases I*, II and III correspond with the orange, white and gray areas, respectively. The solid purple lines are the mixed-ordered and ordered-frozen critical lines for the non-aging version of the model.

$$\begin{aligned} \frac{dx_{k,0}^{\pm}}{dt} &= \sum_{j=0}^{\infty} x_{k,j}^{\mp} \omega_{k,j}^{\mp} - x_{k,0}^{\pm}, \\ \frac{dx_{k,j}^{\pm}}{dt} &= x_{k,j-1}^{\pm} \left(1 - \omega_{k,j-1}^{\pm} \right) - x_{k,j}^{\pm} \quad j > 0. \end{aligned} \quad (11)$$

It can be shown from equation (11) that the stationary solution for the fraction of agents in state $+1$, x_f , obeys the following implicit equation for a complete graph (see appendix B for a detailed explanation):

$$x_f = \frac{F(1 - x_f)}{F(x_f) + F(1 - x_f)}, \quad (12)$$

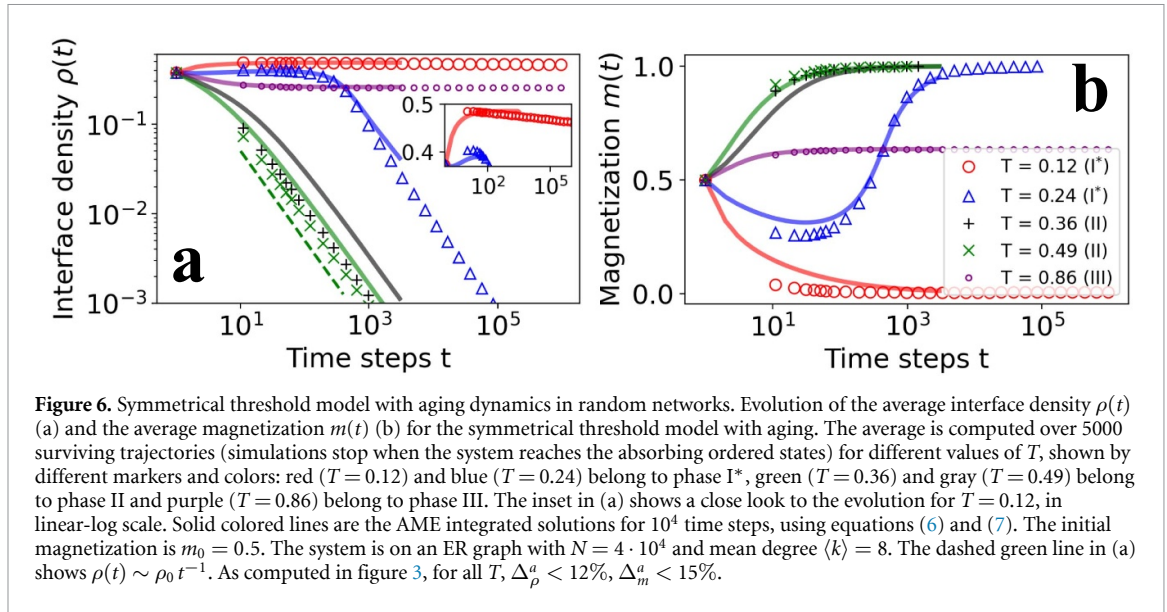
where,

$$F(x) = 1 + \sum_{j=1}^{\infty} \prod_{a=0}^{j-1} \left(1 - p_{\Lambda}(a) \sum_{m=(N-1)T}^{N-1} B_{N-1,m}[x] \right). \quad (13)$$

A solution of equation (12) can be obtained numerically using standard methods, as in [37]. The final magnetization is calculated as $m_f = 2x_f - 1$. With this method, we obtain that the phase diagram for the model with aging is the same as for the original model (refer to figure 1(a)). As a technical point, we note that a truncation of the summation of the variable j in equation (13) is required for the numerical resolution of the implicit equation. The higher the maximum age considered j_{\max} , the higher the accuracy. With $j_{\max} = 5 \cdot 10^4$, the transition lines predicted by this mean-field approach show great accuracy. Moreover, by numerically integrating equation (11), the dynamical evolution of the magnetization and mean internal time can be obtained. Figure 4 shows the agreement between integrated solutions and MC simulations of the system both for the aging and non-aging versions. It should be noted that, while aging introduces only a dynamical delay for the magnetization $m(t)$, the mean internal time $\bar{\tau}(t)$ in phase I shows a different dynamical behavior with aging than in the original model. In this phase, due to the low value of T , the agents selected randomly will change their state (as they fulfill the threshold condition) and reset their internal time. Consequently, while the internal time fluctuates around a stationary value for the original model, when aging is incorporated, due to the activation probability $p_{\Lambda}(j)$ chosen, the mean internal time increases following a recursive relation (equation (C.2)). We refer to appendix C for a derivation of this result.

3.2. Random networks

In contrast to the results obtained in a complete graph, aging effects have a significant impact on the phase diagram of the model on random networks. In figure 5, we show the borders of phase II (first and last value of T where the system reaches the absorbing ordered state for each m_0) obtained from MC simulations running

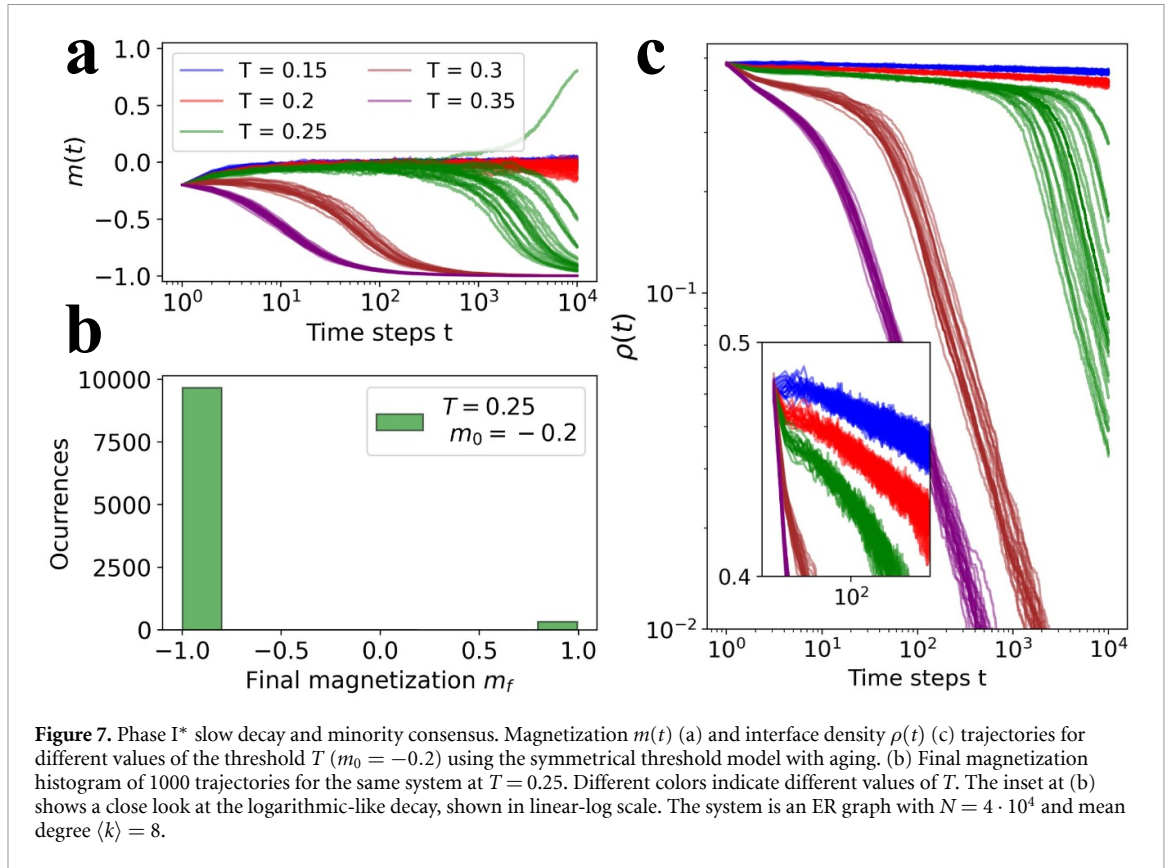


up to a maximum time t_{\max} (dotted colored lines). Reaching the stationary state in this model requires a large number of steps (with a corresponding high computational cost). The two borders of phase II exhibit different behavior as we increase the time cutoff t_{\max} : while the ordered-frozen border does not change with different t_{\max} , the mixed-ordered border is shifted to lower values of T as we increase the time cutoff t_{\max} . Our results suggest that phase I is actually replaced in a good part of the phase diagram by an ordered phase in which the absorbing state $m_f = \pm 1$ is reached after a large number of time steps. Similar results are found for an RR graph (see appendix D). The dependence of the results with t_{\max} calls for a characterization of different phases in terms of dynamical properties rather than by the asymptotic value of the magnetization.

Figure 6 shows the time evolution of our ordering metrics. The dynamical properties are largely affected by the aging mechanism. In terms of the evolution, we find the following regimes:

- **Initial mixing regime (phase I*):** it is characterized by two dynamical transient regimes: a fast initial disordering dynamics followed by a slow ordering process. After the initial fast disordering stage, the average interface density exhibits a very slow (logarithmic-like) decay. Later, due to the finite size of the system, the average interface density follows a power law decay with time, where $\rho(t)$ scales as t^{-1} . This phase exists for the same domain of parameters (m_0 , T) as phase I (orange region in figure 5) in the model without aging (see $T = 0.12, 0.24$ in figure 6).
- **Ordered regime (phase II):** according to the initial majority, the magnetization tends to the ordered absorbing state. This regime is characterized by a power-law interface decay, where $\rho(t)$ scales as t^{-1} . (see $T = 0.36, 0.49$ in figure 6).
- **Frozen regime (phase III):** each individual realization is characterized by an initial tendency toward the majority consensus, but very fast reaches an absorbing frozen configuration (see $T = 0.86$ in figure 6).

The main effect of aging is that the mixed states of phase I are no longer present, at least not for the type of networks that we are analyzing here. We will show later that phase I reemerges in denser graphs. Instead, for sparse graphs, we observe a new phase I* in which the system initially disorders and later orders until reaching the absorbing states $m_f = \pm 1$. This behavior is shown in figure 6 for $T = 0.12$ and 0.26 . For $T = 0.12$, the system initially disorders, and then the interface density follows a logarithmic-like decay (see inset in figure 6(a)). Due to the slow decay, the system stays in this transient regime even after 10^6 time steps, and the fall to the absorbing states is not observed in this figure. Similarly, for $T = 0.26$ the disordering process stops and then the system gradually evolves toward a fully ordered state. For this value of T , the logarithmic-like decay is not appreciated and we just observe the power-law decay due to the finite size of the system. The difference between $T = 0.12$ and $T = 0.26$ comes from the fact that in this phase I*, the interface decay becomes faster as we increase the threshold T (see figures 7(a)–(c)). Notice the different interface decay in figure 7(c) (inset) between values of $T < 0.3$ (phase I*), where all trajectories show a logarithmic-like decay of $\rho(t)$ in a transient regime, and $T \geq 0.3$ (phase II), where trajectories from the initial condition exhibit fast ordering dynamics toward the majority consensus. Moreover, we observe that in phase I*, the initial magnetization m_0 introduces a bias to the stochastic process, implying that the larger m_0 in absolute value, the larger the number of realizations that reach the absorbing state with the same sign of m_0 . However,



the system can still reach the absorbing state of the opposite sign of m_0 (initial minority), as shown in the trajectories with $T = 0.25$ in figure 7(a). Due to the characteristic logarithmic decay of phase I*, a statistical analysis of the inversion process incurs a significant computational cost. In figure 7(b), we present the final magnetization histogram for $T = 0.25$, a value proximal to the I*–II boundary where this analysis is computationally feasible. As depicted in this figure, the proportion of realizations in which consensus is reached in the initial minority state is approximately 3.3%.

In phase II, the system asymptotically orders for any initial condition as in the original model, but the dynamical properties are modified due to the presence of aging: the exponential decay of the interface density is replaced by a slow power-law decay, where the exponents of the exponential and the power-law are found to be similar. Contrary, the dynamical properties of phase III are not affected by the presence of aging. The temporal magnitudes analysis (mean internal time and persistence) can be found in appendix E.

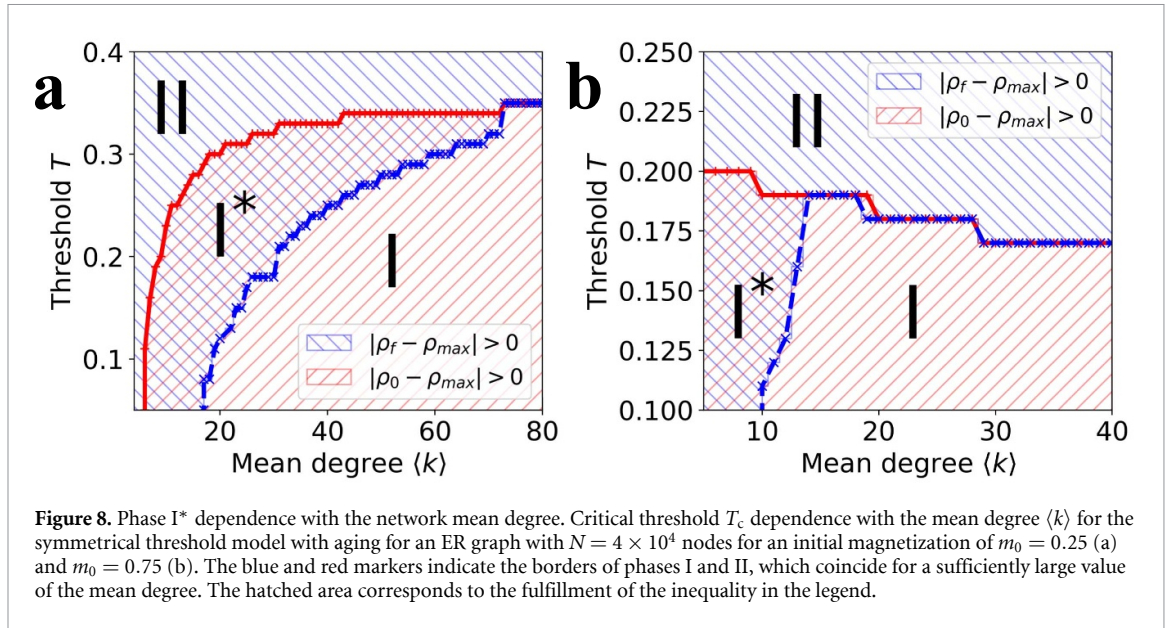
As it occurred for the non-aging version of the model, the dynamical characterization discussed above holds for all possible m_0 except for the symmetric initial condition $m_0 = 0$. The implications of the order–disorder transition (that occurs at a critical mean degree $k_c(N)$) [56] are still present in the model with aging.

To account for the results of our MC simulations, we use the same mathematical framework as described in equation (3). According to the update rules of the symmetrical threshold model with aging, the transition probabilities now depend on the age j , as given by the activation probability $p_A(j)$:

$$\begin{aligned} T_{k,m,j}^+ &= p_A(j) \theta(m/k - T) & T_{k,m,j}^- &= p_A(j) \theta((k-m)/k - T), \\ A_{k,m,j}^\pm &= 1 - T_{k,m,j}^\pm. \end{aligned} \quad (14)$$

We show in figure 5 the mixed-ordered and ordered-frozen transition lines predicted by the integration of the AME equations until a time cutoff t_{\max} . We find good agreement between the theoretical predictions and the simulations both for ER and RR networks (see RR results in appendix D). Regarding dynamical properties, the AME integrated solutions exhibit a remarkable concordance with the evolution of all the metrics as shown in figure 6. Minor discrepancies between the numerical simulations and the integrated solutions are attributed to the different assumptions, discussed previously, on which the AME is based.

The numerical results discussed so far are for random networks with average degree $\langle k \rangle = 8$. According to them and to the analytical insights, one can conclude that aging significantly changes the phase diagram for sparse networks. However, we know that the model with aging shows the same phase diagram as the



model without aging for a fully connected network. This implies that, for ER graphs, as the mean degree $\langle k \rangle$ approaches N , phase I* must disappear. Therefore, the combined effects of increasing the mean degree and introducing aging need to be investigated in more detail. Phase II is distinguishable from phases I and I* because the system initially orders, i.e. $|\rho_0 - \rho_{\max}| = 0$, where ρ_{\max} is the maximum value attained by the interface density during the dynamical evolution. In contrast, Phase I is distinguished from phases I* and II because the system remains disordered, i.e. $|\rho_{\max} - \rho(t_{\max})| \approx 0$. Thus, Phase I* is the only phase among these three where $|\rho_0 - \rho_{\max}| > 0$ and $|\rho_{\max} - \rho(t_{\max})| > 0$. Using this criterion, we studied the dependence of the critical threshold T_c on the mean network degree defining the transition lines between phases I, I*, and II (see figure 8). In the absence of aging, the red line in figure 8 gives the value of the mixed-ordered transition line T_c . When aging is included, at low degree values, phase I is replaced by I*, as expected. However, as the mean degree increases, phase I emerges despite the presence of aging, leading to the coexistence of phases I and I* in the same phase diagram over a range of mean degree values. As the mean degree is further increased, a critical value is reached where phase I* is no longer present, and the discontinuous transition I–II occurs at the same value than in the model without aging. Importantly, this critical mean degree at which phase I* disappears, depends significantly on the initial magnetization m_0 .

4. Symmetrical threshold model in a Moore lattice

We consider next the symmetrical threshold model in a Moore lattice, which is a regular two-dimensional lattice with interactions among nearest and next-nearest neighbors ($k = 8$). From numerical simulations, we obtain a phase diagram (figure 9(a)) that is consistent with our previous results in random networks. The system undergoes a mixed-ordered transition at a threshold value $T_c = 2/8$ which is independent of the value of the initial magnetization m_0 . When $T > 4/8$, the system undergoes an ordered-frozen transition at a critical threshold T_c^* , which depends on m_0 (similarly to what happens in random networks). The final magnetization $m_f(m_0)$ (figure 9(b)) also shows a dependence on m_0 similar to the one found in RR networks (figure 2(c)).

4.1. Original model without aging

Figure 10 shows the results from numerical simulations (for $m_0 = 0$ and 0.5) for the average interface density, the magnetization, and the persistence (the internal time shows the same results as in random graphs). Dynamical properties change significantly for different values of the threshold and initial magnetization m_0 . Similarly to the case of random networks, we find three different regimes corresponding to the three phases, but with some properties different from the results on random networks:

- **Mixed regime (phase I):** it is characterized by fast disordering dynamics with a persistence decay $p(t) \sim \exp(-\ln(t)^2)$, consistent with the results of the Voter model [54]. The interface density and the magnetization exhibit fast dynamics toward their asymptotic values in the dynamically active stationary state (see $T = 1/8, 2/8$ in figure 10).

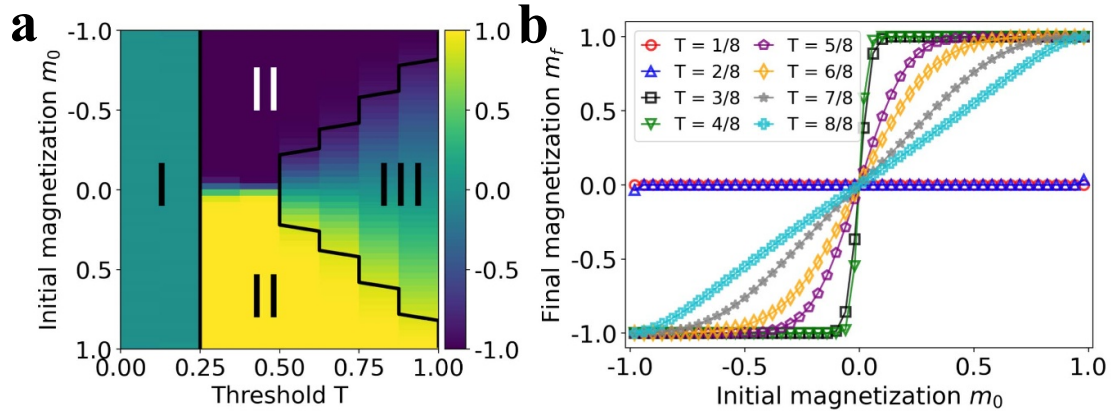


Figure 9. Symmetrical threshold model in a Moore lattice. (a) Phase diagram of the symmetrical threshold model in a Moore lattice of size $N = L \times L$, with $L = 100$. The color map indicates the value of the average final magnetization m_f . Solid black lines are the borders of phase II (first and last value of T where the system reaches the absorbing ordered state for each m_0), computed from the numerical simulations. (b) Average final magnetization m_f as a function of the initial magnetization m_0 for the discrete values of the threshold T (indicated with different colors and markers) in a Moore lattice of the same size. Average performed over 5000 realizations.

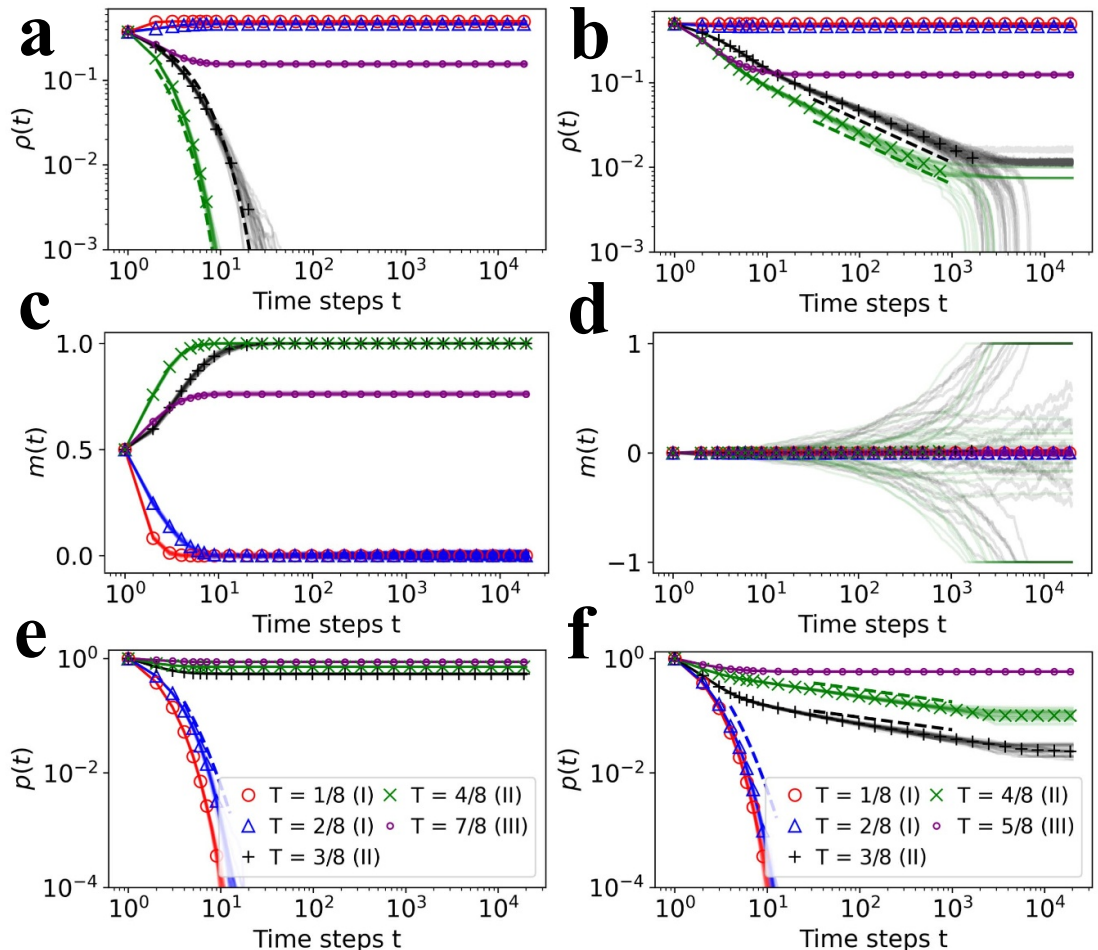


Figure 10. Dynamical regimes in a Moore lattice. Evolution of the average interface density $\rho(t)$ (a) and (b), the average magnetization $m(t)$ (c) and (d), and the persistence $p(t)$ (e) and (f) for the symmetrical model in a Moore lattice starting from a random configuration with $m_0 = 0.5$ (a, c, e) and $m_0 = 0$ (b, d, f). We plot 50 different trajectories in solid lines and the average of 5000 surviving trajectories (simulations stop when the system reaches the absorbing ordered states) in different markers. Different colors and markers indicate different threshold values: red ($T = 1/8$) and blue ($T = 2/8$) belong to phase I, green ($T = 3/8$) and black ($T = 4/8$), and purple ($T = 5/8, 7/8$) belong to phase III. The average magnetization $m(t)$ is computed according to the two symmetric absorbing states. System size is fixed at $N = L \times L$, $L = 200$. The dashed lines in (a) are $\rho \sim \exp(-\alpha \cdot t)$ with $\alpha = 0.5$ (black) and $\alpha = 0.8$ (green), in (b) are $\rho(t) \sim at^{-1/2}$ with $a = 0.36$ (black) and $a = 0.2$ (green), in (e) and (f) is $p(t) \sim \exp(-\ln(t)^2)$ (blue).

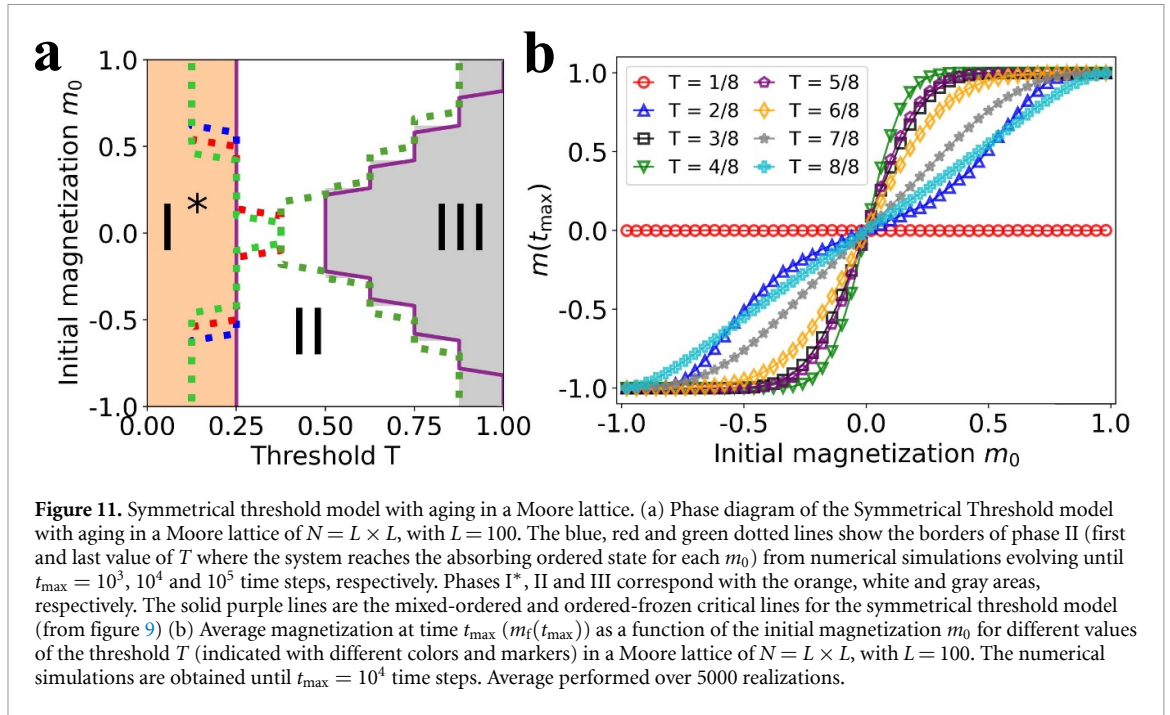


Figure 11. Symmetrical threshold model with aging in a Moore lattice of $N = L \times L$, with $L = 100$. The blue, red and green dotted lines show the borders of phase II (first and last value of T where the system reaches the absorbing ordered state for each m_0) from numerical simulations evolving until $t_{\max} = 10^3, 10^4$ and 10^5 time steps, respectively. Phases I*, II and III correspond with the orange, white and gray areas, respectively. The solid purple lines are the mixed-ordered and ordered-frozen critical lines for the symmetrical threshold model (from figure 9) (b) Average magnetization at time t_{\max} ($m_f(t_{\max})$) as a function of the initial magnetization m_0 for different values of the threshold T (indicated with different colors and markers) in a Moore lattice of $N = L \times L$, with $L = 100$. The numerical simulations are obtained until $t_{\max} = 10^4$ time steps. Average performed over 5000 realizations.

- **Ordered regime (phase II):** it is characterized by an exponential or power-law decay of the interface density, depending on the initial condition (see details below). The magnetization tends to the absorbing ordered state (see $T = 3/8, 4/8$ in figure 10).
- **Frozen regime (phase III):** it is characterized by an initial ordering process, but the system freezes fast (see $T = 5/8$ in figure 10).

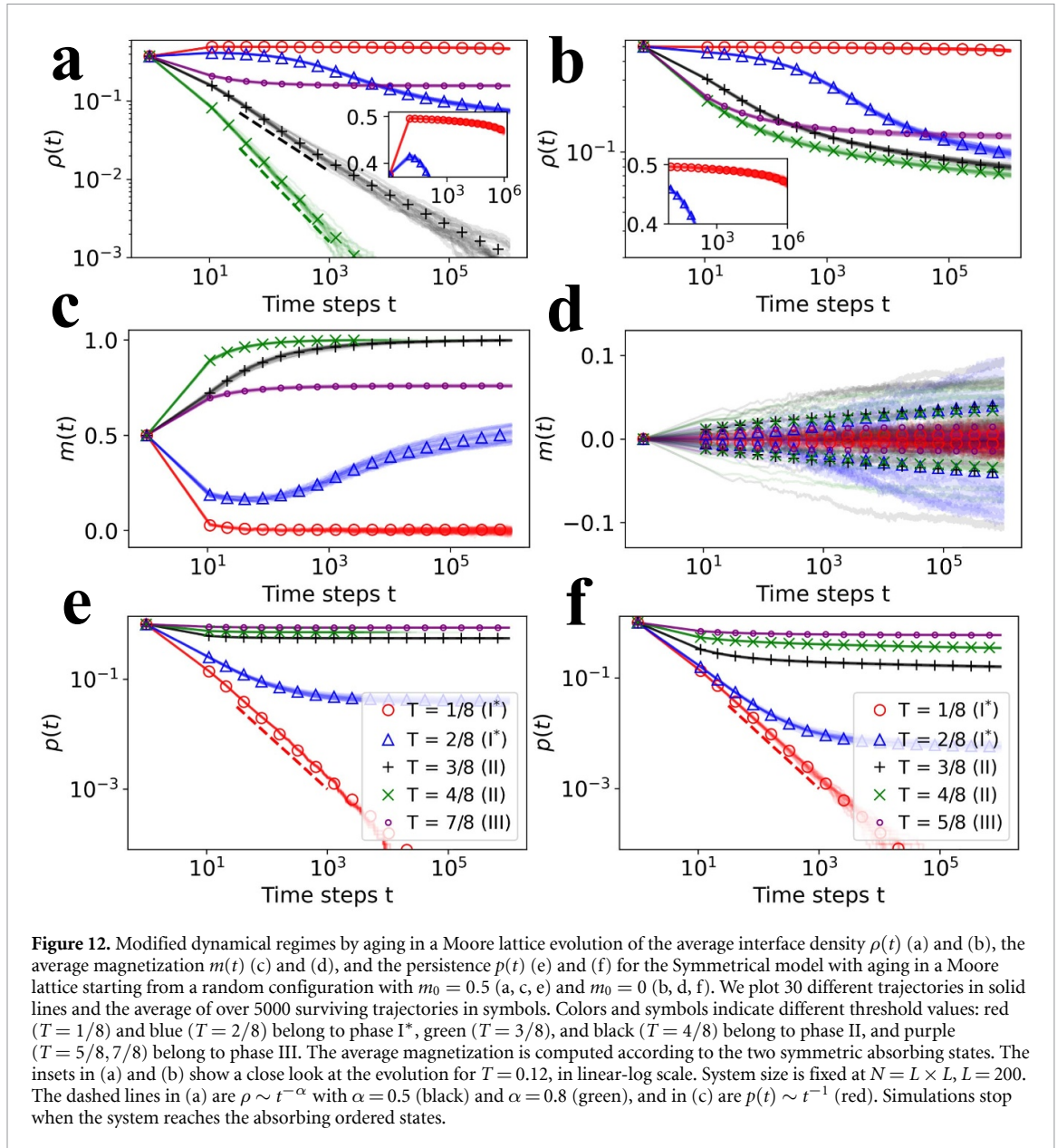
In particular, in phase II for $m_0 = 0$ the persistence and interface density decay are found to decay as a power law, $p(t) \sim t^{-0.22}$ and $\rho(t) \sim t^{-1/2}$, respectively (consistent with the results of the Ising model [57–60]). For a biased initial condition ($m_0 = 0.5$), $p(t)$ decays to the initial majority fraction (which corresponds to the state reaching consensus), and $\rho(t)$ follows an exponential-like decay. Note that, for $m_0 = 0$, not all trajectories reach the ordered absorbing states ($m_f = \pm 1$). There exist other absorbing configurations as, for example, a flat interface configuration for $T = 4/8$, no agent will be able to change, and the system remains trapped in this state. This result is not observed for $m_0 > 0$.

Contrary, phases I and III show similar dynamics for balanced ($m_0 = 0$) and unbalanced ($m_0 = 0.5$) initial conditions. In phase I, the system shows disordering dynamics with a persistence decay similar to the one exhibited for the Voter model in a lattice [54] while in phase III, the system exhibited freezing dynamics with an initial tendency toward the majority consensus.

Due to the lattice structure and high clustering, the mathematical tools employed in the previous sections for random networks are inapplicable to regular lattices. Consequently, we limit ourselves to the results of numerical simulations. On the other hand, a regular structure facilitates easy modification of the geometry structure of the initial condition. Appendix F presents an analysis of how a compact initial condition influences the dynamics of the symmetrical threshold model (and its variant with aging).

4.2. The role of aging

We show in figure 11(a) the borders of phase II obtained from numerical simulations running up to a time t_{\max} (dotted colored lines). Similarly to the behavior observed in random networks, the mixed-ordered border is shifted to lower values of T as we increase the simulation time cutoff t_{\max} . Thus, phase I is replaced by an ordered phase due to the aging mechanism. Examining the dependence of the final value of the magnetization on its initial condition $m_f(m_0)$ (figure 11(b)), one can conclude that the mixed phase is still present, at least transiently, as in the initial disordering phase described in the previous section (phase I*). Phase II is again characterized by an asymptotically ordered state where the initial majority reaches consensus. However, for this specific structure, near $m_0 = 0$ and $T = 1/2$, the ordered state is not reached for any threshold value. Furthermore, comparing with figure 11(b) with the results from the model without aging (figure 9(b)), the discontinuous jump at $m_0 = 0$ for $T = 3/8, 4/8$ is replaced by a continuous transition, where a range of states with $0 < |m_f| < 1$ are present around $m_0 = 0$. To determine whether these states



belong to phases I*, II or III, we need again a characterization of phases in terms of dynamical properties. According to the results in figure 12, we find here the same regimes identified for random networks:

- **Initial mixing regime (phase I*):** after the initial disordering stage, the average interface density shows a very slow decay reflecting the slow growth of spatial domains in each binary state. The persistence in this phase shows a power-law decay $p(t) \sim t^{-1}$ (see $T = 1/8, 2/8$ in figure 12).
- **Ordered regime (phase II):** it is characterized by coarsening dynamics that end in the absorbing states $m_f = \pm 1$. The form of the decay of the interface density depends on the value of m_0 (see $T = 3/8, 4/8$ in figure 12).
- **Frozen regime (phase III):** it is characterized by an initial tendency to order but the system very fast reaches an absorbing frozen configuration (see $T = 5/8, 7/8$ in figure 12).

The implications of aging become explicit by comparing the dynamical properties of the cases with aging (figure 12) and without aging (figure 10). When the threshold is $T < 3/8$, phase I is replaced by phase I* in which there is an initial disordering process very fast followed by a slow coarsening process that accelerates when we increase the threshold. Although the aging implications in this phase are similar to those observed in the ER graph, the coarsening process is slower (see insets in figures 12(a) and (b)).

In phase II ($T = 3/8, 4/8$) and when $m_0 = 0.5$, the system exhibits coarsening toward the ordered state $m_f = \pm 1$. In this case, the interface decay $\rho \sim \exp(-\alpha t)$, observed in the absence of aging is replaced, due to aging, by a power law decay $\rho \sim t^{-\alpha}$, as noted in [42]. We find $\alpha = 0.5$ and 0.8 for $T = 3/8$ and $4/8$,

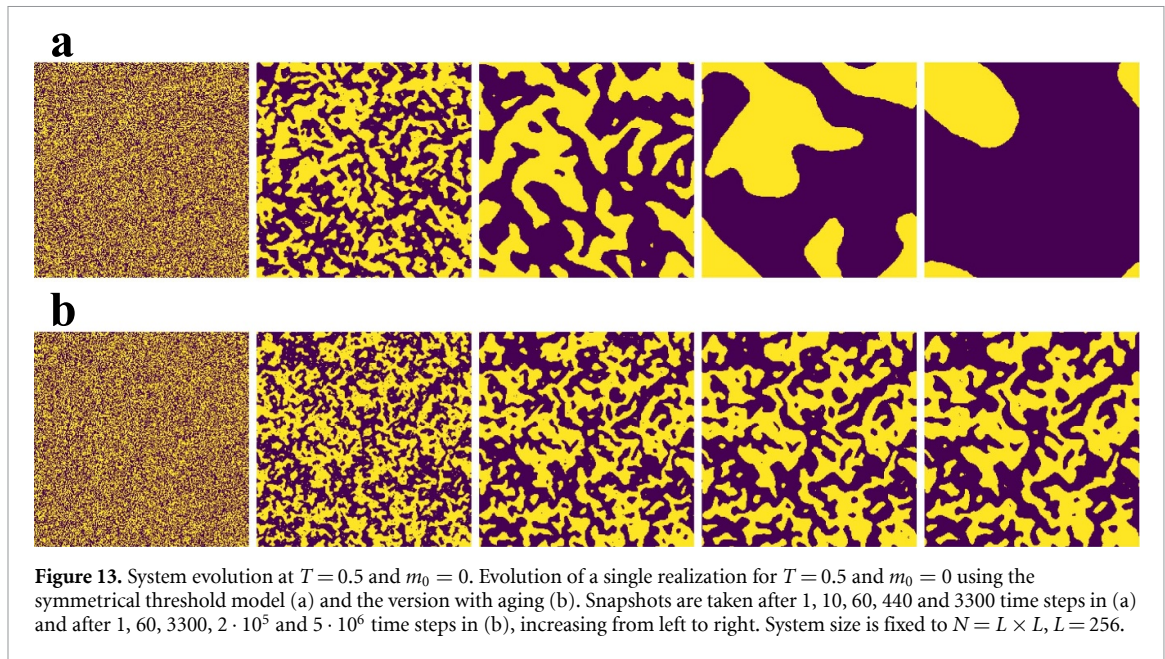


Figure 13. System evolution at $T = 0.5$ and $m_0 = 0$. Evolution of a single realization for $T = 0.5$ and $m_0 = 0$ using the symmetrical threshold model (a) and the version with aging (b). Snapshots are taken after 1, 10, 60, 440 and 3300 time steps in (a) and after 1, 60, 3300, $2 \cdot 10^5$ and $5 \cdot 10^6$ time steps in (b), increasing from left to right. System size is fixed to $N = L \times L$, $L = 256$.

respectively. For $m_0 = 0$, the power law decay of the interface density vanishes with aging, and the system exhibits coarsening dynamics much slower than for an unbalanced initial condition. In this region of the phase diagram, spatial clusters start to grow from the initial condition, but once formed, it takes a long time for the system to reach the absorbing state $m_f = \pm 1$. We note that for these parameter values, the system is not able to reach $|m|$ over 0.1 even after 10^6 time steps, but since there is coarsening from the initial condition, the expected stationary state as $t \rightarrow \infty$ is $m_f = \pm 1$. There is neither initial disordering nor freezing, these values correspond to the defined phase II, even though the system exhibits ‘long-lived segregation’ long transient dynamics (see the difference with the dynamics of the model without aging in figure 13). In figure 11(a), we differentiate phase II from phase III by analyzing the activity in the system: if agents are changing, even though the interface decay is slow, the system is in phase II. If agents are frozen, it lies in phase III. When comparing the ordered–frozen critical line to the one from the original model (purple line), we notice that aging causes certain values (m_0, T) that were previously in phase II near the critical line to enter the frozen phase.

Finally, it should be noted that in phase I*, the initial disordering dynamics drive the system toward $m = 0$. Therefore, the subsequent coarsening dynamics follow the slow interface decay observed in phase II for $m_0 \sim 0$. Thus, the presence of aging implies that the system asymptotically orders for any initial condition, but due to the initial disordering, the coarsening dynamics fall into the ‘long-lived segregation’ regime independently of the initial condition.

5. Summary and conclusions

In this work, we have studied with MC numerical simulations and analytical calculations the symmetrical threshold model. In this model, the agents, nodes of a contact network, can be in one of the two symmetric states ± 1 . System dynamics follows a complex contagion process in which a node changes state when the fraction of neighboring nodes in the opposite state is above a given threshold T . For $T = 1/2$, the model reduces to a majority rule or the zero temperature spin flip kinetic Ising model. When the change of state is only possible in one direction, say from 1 to -1 , it reduces to the Granovetter–Watts Threshold model [9, 12, 42]. We have considered the cases of a fully connected network, ER, and RR networks, as well as a regular two-dimensional Moore lattice.

We have found that, in the parameter space of threshold T and initial magnetization m_0 , the model exhibits three distinct phases, namely phase I or mixed, phase II or ordered, and phase III or frozen. The existence of these three phases is robust for different network structures. These phases are well characterized by the final state (m_f), and by dynamical properties such as the interface density $\rho(t)$, time-dependent average magnetization $m(t)$, persistence times $p(t)$, and mean internal time $\bar{\tau}(t)$. These phases can be obtained analytically in the mean-field case of a fully connected network. For the random networks considered, we derive an AME [42, 50] considering agents in each state according to their degree k , neighbors in state -1 , m , and age j . From this AME, we have also derived an HMF approximation. While the AME

reproduces with great accuracy the results of MC numerical simulations of the model (both static and dynamic), the HMF shows an important lack of agreement, highlighting the importance of high-accuracy methods necessary for threshold models.

Aging is incorporated in the model as a decreasing probability to modify the state as the time already spent by the agent in that state increases. The key finding is that the mixed phase (phase I), characterized by an asymptotically disordered dynamically active state, does not always exist: the aging mechanism can drive the system to an asymptotic absorbing ordered state, regardless of how low the threshold T is set. A similar effect of aging was already described for the Schelling model in [41]. When the dynamics are examined in detail, a new phase I^* , defined in terms of dynamical properties, emerges in the domain of parameters where the model without aging displays phase I. This phase is characterized by an initial disordering regime ($m \rightarrow 0$) followed by a slow ordering dynamics, driving the system toward the ordered absorbing states (including the one with spins opposite to the majoritarian initial option). This result is counter-intuitive since aging incorporates memory into the system, yet in this phase, the system ‘forgets’ its initial state. The network structure plays an important role in the emergence of phase I^* since it does not exist for complete graphs. A detailed analysis reveals that phase I^* replaces phase I only for sparse networks, including the case of the Moore lattice. For ER networks we find that, as the mean degree increases, phase I reappears and there is a range of values of the mean degree for which phases I and I^* coexist. Beyond a critical value of the mean degree, phase I extends over the entire domain of parameters where phase I^* was observed.

While aging favors reaching an asymptotic absorbing ordered state for low values of T (phase I), in phase II the ordering dynamics are slowed down by aging, changing, both in random networks and in the Moore lattice, the exponential decay of the interface density by a power law decay with the same exponent. The aging mechanism is found not to be important in the frozen phase III. All these effects of aging in the three phases are well reproduced for random networks by the AME derived in this work, which is general for any chosen activation probability $p_A(j)$.

For the Moore lattice, we have also considered in detail the special case of the initial condition $m_0 = 0$. In this case, phase I^* emerges, and phase III is robust against aging effects. However, in phase II aging destroys the characteristic power law decay of the interface density, $\rho(t) \sim at^{-1/2}$, associated with curvature reduction of domain walls. This would be a main effect of aging in the dynamics of the phase transition for the zero temperature spin flip kinetic Ising model [61]. Additionally, this regular structure allowed us to analyze the effects of a compact initial condition. We have shown that the joint effect of aging and a compact initial condition prevent the ordered phases from reaching the consensus state (see appendix F).

As a final remark on the general effects of aging in different models of collective behavior, we note that the replacement of a dynamically active disordered stationary phase by a dynamically ordering phase is generic. In this paper, we find the replacement of phase I by phase I^* . Likewise in the Voter model, aging destroys long-lived dynamically active states characterized by a constant value of the average interface density, and it gives rise to coarsening dynamics with a power law decay of the average interface density [34]. In the same way, in the Schelling segregation model, a dynamically active mixed phase is replaced, due to the aging effect, by an ordering phase with segregation in two main clusters. Another aging effect that seems generic, in phases in which the system orders when there is no aging, is the replacement of dynamical exponential laws by power laws. This is what happens here in phase II for the decay of the average interface density but, likewise, exponential cascades in the Granovetter–Watts model are replaced due to aging by a power-law growth with the same exponent [42].

Further research with the general AME used in this study would involve a new approach that considers the master equation, as described in [62]. This approach aims to incorporate finite size effects, which are relevant when m_0 is close to zero, and would provide a mathematical framework for further analysis of the results in [56]. Regarding the model, this article reports the main features of the symmetrical threshold model dynamics and the aging effects. However, there are several areas for future research along this lines, such as investigating the impact of strongly heterogeneous [63] or coevolving networks [64, 65], exploring the dependence of the results on the aging activation function p_A , and examining the joint effect of aging and strongly heterogeneous degree distributions.

Data availability statement

Any data that support the findings of this study are included within the article.

Acknowledgment

Financial support has been received from the Agencia Estatal de Investigación (AEI, MCI, Spain) MCIN/AEI/10.13039/501100011033 and Fondo Europeo de Desarrollo Regional (UE) under Project

APASOS (PID2021-122256NB-C21 and PID2021-122256NB-C22) and the María de Maeztu Program for units of Excellence, Grant CEX2021-001164-M).

Appendix A. Heterogeneous mean-field

When the transition and aging probabilities do not depend on j , $T_{k,m,j}^\pm = T_{k,m}^\pm$ and $A_{k,m,j}^\pm = A_{k,m}^\pm$, if we are not interested in the solutions $x_{k,m,j}^\pm(t)$ and we just want the final magnetization, equation (3) is reduced to Gleeson’s AME [50] by summing variable j . If we truncate the degree distribution at a reasonable large degree k_{\max} , Gleeson’s AME is a system of $(k_{\max} + 1)(k_{\max} + 1)$ differential equations without loss of accuracy.

Moreover, following the steps in [50], we perform a heterogeneous mean-field (HMF) approximation to reduce our system to $k_{\max} + 1$ differential equations:

$$\frac{d}{dt}x_k^- = -x_k^- \sum_{m=0}^k T_{k,m}^- B_{k,m}[\omega] + (1 - x_k^-) \sum_{m=0}^k T_{k,m}^+ B_{k,m}[\omega], \tag{A.1}$$

where $x_k^- = \sum_j \sum_m x_{k,m,j}^-$ and $\omega = \sum_k p_k \frac{k}{z} x_k^-$. This system of differential equations, coupled via ω , cannot be solved analytically. Solving numerically with standard methods, HMF predicts a mixed-ordered transition line that qualitatively captures the critical line dependence but quantitatively differs from the numerical simulations (see the red dashed line in figures 2(a) and (b) and the dotted colored lines in figure 2(c). Moreover, this approximation does not predict a frozen phase in any of the networks considered. Instead, for high values of T , the integrated stationary solutions are always $m_f = \pm 1$, regardless of m_0 . From this analysis, we conclude that we need sophisticated methods beyond an HMF description to describe the symmetrical threshold model’s phase diagram (in a random sparse network), as occurs for the asymmetrical Granovetter–Watts’ threshold model (see [42]). The accuracy of the HMF approximation increases when we approach the complete graph scenario $\langle k \rangle / N \rightarrow 1$.

Appendix B. Derivation of the stationary solution via the HMF taking into account aging

Setting the time derivatives to 0 in equations (11), we obtain the relations for the stationary state:

$$x_{k,0}^\pm = \sum_{j=0}^\infty x_{k,j}^\mp \omega_{k,j}^\mp, \tag{B.1}$$

$$x_{k,j}^\pm = x_{k,j-1}^\pm (1 - \omega_{k,j-1}^\pm) \quad j > 0,$$

from where we extract the stationary condition $x_{k,0}^- = x_{k,0}^+$, as in [37]. Notice that by setting $p_A(j) = 1$ and summing over all ages j , we recover the HMF approximation (equation (A.1)) for the model without aging. Defining $x_j^\pm(t)$ as the fraction of agents in state ± 1 with age j :

$$x_j^\pm = \sum_k p_k x_{k,j}^\pm, \tag{B.2}$$

and using the degree distribution of a complete graph $p_k = \delta(k - N + 1)$ (where $\delta(\cdot)$ is the Dirac delta), we sum over the variable k and rewrite equation (B.1) in terms of x_j^\pm :

$$x_0^\pm = \sum_{j=0}^\infty x_j^\mp \omega_j^\mp, \tag{B.3}$$

$$x_j^\pm = x_{j-1}^\pm (1 - \omega_{j-1}^\pm) \quad j > 0,$$

where $\omega_j^\pm \equiv \omega_{N-1,j}^\pm$. Note that the stationary condition $x_0^- = x_0^+$ remains valid after summing over the degree variable. We compute the solution x_j^\pm recursively as a function of x_0^\pm :

$$x_j^\pm = x_0^\pm F_j^\pm \quad \text{where} \quad F_j^\pm = \prod_{a=0}^{j-1} (1 - \omega_a^\pm), \tag{B.4}$$

and summing all j ,

$$x^\pm = x_0^\pm F^\pm \quad \text{where} \quad F^\pm = 1 + \sum_{j=1}^{\infty} F_j^\pm. \quad (\text{B.5})$$

Using the stationary condition $x_0^- = x_0^+$, we reach:

$$\frac{x^+}{x^-} = \frac{F^+}{F^-}. \quad (\text{B.6})$$

Notice that, for the complete graph, $\tilde{x}^+ = x$, $\tilde{x}^- = 1 - x$. Therefore, F^\pm is a function of the variable x^\mp ($F^+ = F(1 - x)$). Thus, we rewrite the previous expression just in terms of the variable x :

$$\frac{x}{1 - x} = \frac{F(1 - x)}{F(x)}. \quad (\text{B.7})$$

Appendix C. Internal time recursive relation in phase I/I*

In phases I and I*, the exceeding threshold condition ($m/k > T$) is full-filled for almost all agents in the system. Thus, agents will change their state and reset the internal time once activated. For the original model, all agents are activated once in a time step on average, but for the model with aging, the activation probability plays an important role. We consider here a set of N agents that are activated randomly with an activation probability $p_A(j)$ and, once activated, they reset their internal time. Being $n_i(t)$ the fraction of agents with internal time i at the time step t , we build a recursive relation for the previously described dynamics in terms of variables i and t :

$$\begin{aligned} n_1(t) &= \sum_{i=1}^{t-1} p_A(i) n_i(t-1) \\ n_i(t) &= (1 - p_A(i-1)) n_{i-1}(t-1) \quad i > 1. \end{aligned} \quad (\text{C.1})$$

This recursion relation can be solved numerically from the initial condition ($n_1(0) = 1$, $n_i(0) = 0$ for $i > 1$). To obtain the mean internal time at time t , we just need to compute the following:

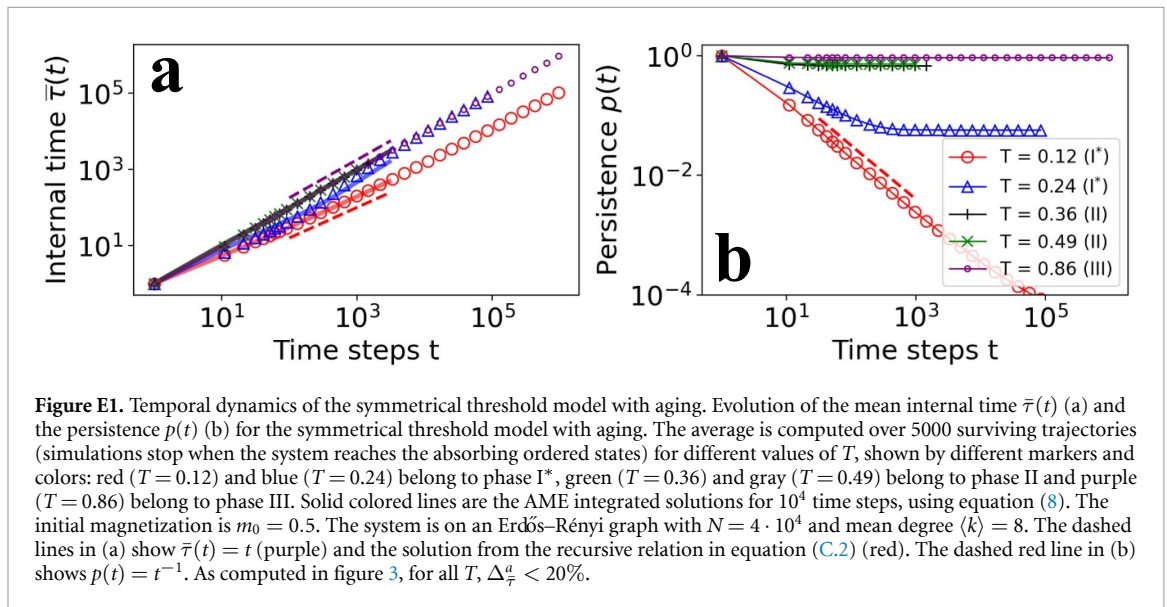
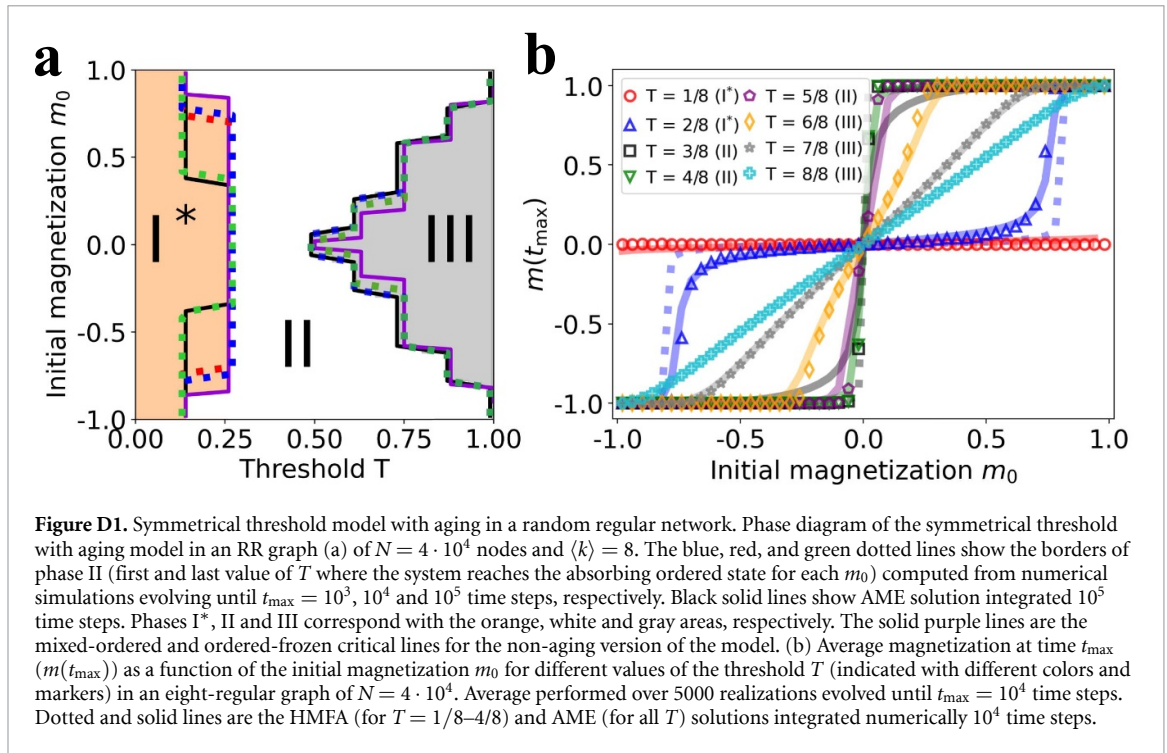
$$\bar{\tau}(t) = \sum_{i=1}^t i n_i(t). \quad (\text{C.2})$$

The solution from this recursive relation describes the mean internal time dynamics with great agreement with the numerical simulations performed at phase I (for the complete graph) and phase I* (for the Erdős–Rényi and Moore lattice).

Appendix D. Symmetrical threshold model with aging in random-regular graphs

Figure D1 shows the borders of phase II (first and last value of T where the system reaches the absorbing ordered state for each m_0) obtained from Monte Carlo simulations running up to a maximum time t_{\max} (dotted colored lines) for an RR graph. Reaching the stationary state in this model requires a large number of steps and it has a high computational cost. The two borders of phase II exhibit different behavior as we increase the maximum number of time steps t_{\max} : while the ordered-frozen border does not change with different t_{\max} , the mixed-ordered border is shifted to lower values of T as we increase the simulation time cutoff t_{\max} . As it occurs for the results in ER graphs (figure 5), our results suggest that phase I is actually replaced in a good part of the phase diagram by an ordered phase in which the absorbing state $m_f = \pm 1$ is reached after a large number of time steps. The ordered-frozen border is now slightly shifted to lower values of the threshold T due to aging. Figure D1(b) shows the average magnetization on RR graphs with simulations running up to a time $t_{\max} = 10^4$. Upon comparison with figure 2(c), the dependence on m_0 is quite similar, indicating the persistence of a transient mixed phase. This calls for a characterization of different phases in terms of dynamical properties and not only by the asymptotic value of the magnetization.

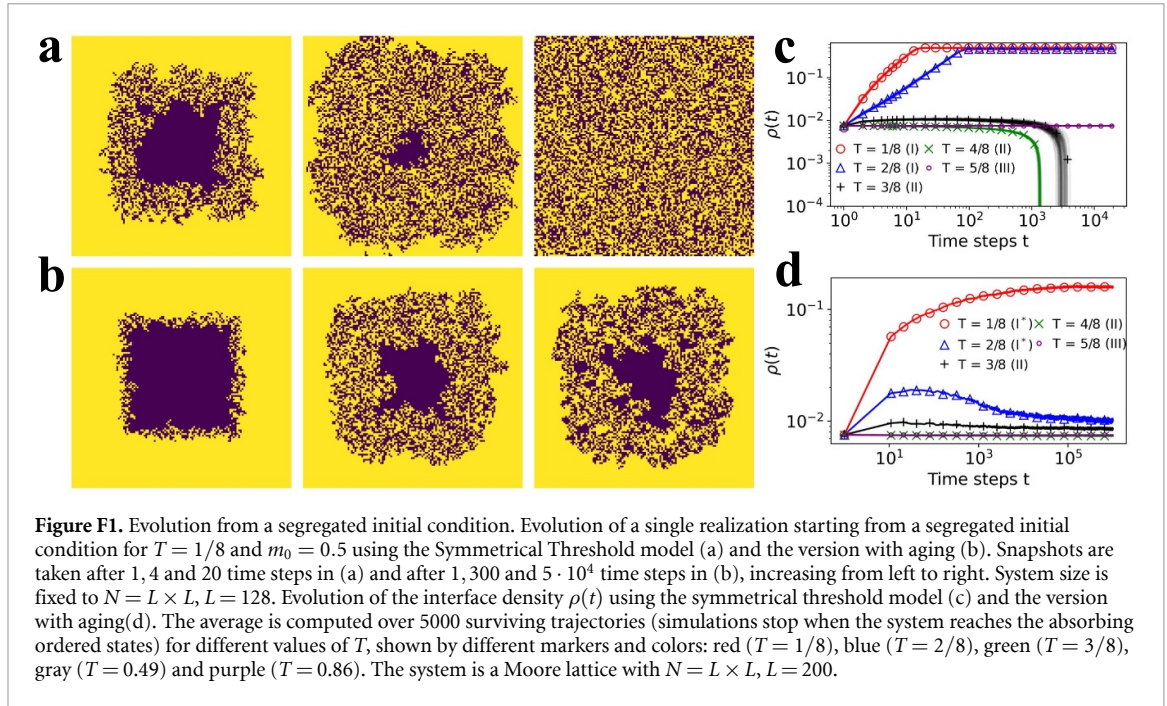
Regarding to the AME integrated solutions, figure D1 shows the mixed-ordered and ordered-frozen transition lines predicted by the integration of the AME equations until a time cutoff t_{\max} , which show a good agreement with the numerical simulations. Figure D1(b) also shows the predicted dependence of $m_f(m_0)$ for the RR graph. For comparison purposes, the numerical integration is computed until the highest t_{\max} used in the Monte Carlo simulations. In addition, we apply the previously introduced HMF taking into account aging (HMFA) to these random networks by numerically integrating equations (11). The results,



displayed as dotted colored lines in figure D1(b), show similarity to the AME solution for $T < 0.5$. Nevertheless, as it occurred for the HMF in the original model, this mathematical framework is not able to describe the frozen phase.

Appendix E. Temporal dynamics in the symmetrical threshold model with aging

Figure E1 shows the evolution of the temporal dynamics via the mean internal time and the persistence. The persistence in phase I* shows a power-law decay, where $p(t)$ scales as t^{-1} , and the internal time shows an increase following the recursive relation given in equation (C.2), as it occurred for the mean-field scenario (figure 4). On the other hand, in phase II, the persistence decays from 1 to the fraction of nodes of the initial majority (the one that does not change state and reaches consensus) and the mean internal time scales linearly with time, $\bar{\tau}(t) \sim t$. For the internal time, the AME integrated solutions exhibit a remarkable concordance with the numerical simulations. Minor discrepancies between the numerical simulations and the integrated solutions can be attributed to the assumption of an infinitely sized system in the AME. As it occurred for the model without aging, the persistence cannot be predicted by this framework.



Appendix F. Joint effect of aging and a segregated initial condition in a lattice

So far, we have analyzed the dynamics of the symmetrical threshold model (with and without aging) starting from a random initial condition with magnetization m_0 . However, a segregated initial condition, in which nodes on the same state are clustered together, may affect the dynamical behavior. In this appendix, we run numerical simulations starting with a segregated initial condition. In our system of side L , the segregated initial condition consists of a centered square of agents with state -1 (of side $L/4$), surrounded by agents in state $+1$. Therefore, the initial magnetization is $m_0 = 0.5$.

Firstly, due to the geometry of the initial condition, any value of $T > 5/8$ remains trapped at the initial condition, as no agent in the system will have their threshold exceeded. Consequently, all values of $T > 5/8$ fall under phase III (frozen phase). This phenomenon occurs for both the aging and non-aging versions of the model.

The interesting behavior occurs at $T < 5/8$. In figure F1(c), we present the evolution of the interface density for the symmetrical threshold model (without aging). The three phases of the model found starting from a random configuration, are robust (at the same values of T): the system tends toward a mixed active state in phase I ($T = 1/8, 2/8$), tends toward the ordered state according to the initial majority in phase II ($T = 3/8, 4/8$) and freezes in phase III ($T > 5/8$). Nevertheless, the dynamics toward the final state differ from the results in section 4. Specifically, at $T = 3/8$ and $4/8$, due to the initial segregated condition, the system remains trapped in a transient segregated state for more than 10^3 time steps. In phase I ($T = 1/8, 2/8$), the disordered domains grow from the interface (of the segregated initial condition) until it fills the whole system (see figure F1(a)).

When aging is included (figure F1(d)), the dynamical regimes are similar to the ones starting from an initial random condition: the system exhibits an initial disordering followed by coarsening dynamics in phase I* ($T = 1/8, 2/8$), tends toward order (but gets trapped into a ‘long-lived’ transient regime) in phase II ($T = 3/8, 4/8$) and freezes at phase III ($T > 5/8$). A segregated initial condition favors that agents in the bulk of the system do not get activated because they never exceed the threshold condition and the internal time keeps growing at each time step. As it occurred starting from an initial random condition at $m_0 = 0$ (see figure 12(b)), for $T = 3/8, 4/8$ (phase II) the system gets trapped into a ‘long-lived segregated’ transient state (favored by the initial condition), preventing the system from reaching an ordered state.

For $T = 1/8, 2/8$ (phase I*), the system exhibits an initial disordering followed by slow coarsening dynamics. For $T = 2/8$, figure F1(d) shows that the interface initially increases, but, after a few time steps, starts to slowly decrease, while for $T = 1/8$, we only see the initial disordering transient state. Figure F1(b) shows for $T = 1/8$ the emergence of small ordered clusters within the disordered region of the system (after several time steps) due to the presence of aging.

To summarize, the main effect of a segregated initial condition (in comparison with the random initial condition) is to trap the system into a transient segregated state at the ordering phases (phase II in the

non-aging version and phases I* and II in the aging version). In addition, aging favors this transient segregated state, leading the system into a slow-ordering dynamical regime.

ORCID iD

David Abella  <https://orcid.org/0000-0002-0079-5689>

References

- [1] Castellano C, Fortunato S and Loreto V 2009 *Rev. Mod. Phys.* **81** 591–646
- [2] Jusup M et al 2022 *Phys. Rep.* **948** 1–148
- [3] Bianconi G et al 2023 *J. Phys. Complex.* **4** 010201
- [4] Liggett T M et al 1999 *Stochastic Interacting Systems: Contact, Voter and Exclusion Processes* vol 324 (Springer)
- [5] Sood V and Redner S 2005 *Phys. Rev. Lett.* **94** 178701
- [6] Suchecki K, Eguíluz V M and San Miguel M 2005 *Phys. Rev. E* **72** 036132
- [7] Fernández-Gracia J, Suchecki K, Ramasco J J, San Miguel M and Eguíluz V M 2014 *Phys. Rev. Lett.* **112** 158701
- [8] Redner S 2019 *C. R. Phys.* **20** 275–92
- [9] Granovetter M 1978 *Am. J. Sociol.* **83** 1420–43
- [10] Pastor-Satorras R, Castellano C, Van Mieghem P and Vespignani A 2015 *Rev. Mod. Phys.* **87** 925–79
- [11] Gleeson J P 2011 *Phys. Rev. Lett.* **107** 068701
- [12] Watts D J 2002 *Proc. Natl Acad. Sci.* **99** 5766–71
- [13] Centola D, Eguíluz V M and Macy M W 2007 *Physica A* **374** 449–56
- [14] Centola D 2018 *Science* **361** 1320–1320
- [15] Gleeson J P and Cahalane D J 2007 *Phys. Rev. E* **75** 056103
- [16] Hackett A, Melnik S and Gleeson J P 2011 *Phys. Rev. E* **83** 056107
- [17] Hackett A and Gleeson J P 2013 *Phys. Rev. E* **87** 062801
- [18] Gleeson J P 2008 *Phys. Rev. E* **77** 046117
- [19] de Arruda G F, Petri G and Moreno Y 2020 *Phys. Rev. Res.* **2** 023032
- [20] Diaz-Diaz F, San Miguel M and Meloni S 2022 *Sci. Rep.* **12** 9350
- [21] Min B and San Miguel M 2023 *Entropy* **25** 929
- [22] de Oliveira M J 1992 *J. Stat. Phys.* **66** 273–81
- [23] Pereira L F and Moreira F B 2005 *Phys. Rev. E* **71** 016123
- [24] Campos P R, de Oliveira V M and Moreira F B 2003 *Phys. Rev. E* **67** 026104
- [25] Castellano C, Mu noz M A and Pastor-Satorras R 2009 *Phys. Rev. E* **80** 041129
- [26] Mobilia M 2015 *Phys. Rev. E* **92** 012803
- [27] Mellor A, Mobilia M and Zia R 2016 *Europhys. Lett.* **113** 48001
- [28] Min B and San Miguel M 2017 *Sci. Rep.* **7** 12864
- [29] Jedrzejewski A 2017 *Phys. Rev. E* **95** 012307
- [30] Peralta A F, Carro A, San Miguel M and Toral R 2018 *Chaos* **28** 075516
- [31] Nowak B and Sznajd-Weron K 2019 *Complexity* **2019** 1–14
- [32] Nowak B and Sznajd-Weron K 2020 *Phys. Rev. E* **101** 052316
- [33] Stark H U, Tessone C J and Schweitzer F 2008 *Phys. Rev. Lett.* **101** 018701
- [34] Fernández-Gracia J, Eguíluz V M and San Miguel M 2011 *Phys. Rev. E* **84** 015103
- [35] Pérez T, Klemm K and Eguíluz V M 2016 *Sci. Rep.* **6** 21128
- [36] Boguñá M, Lafuerza L F, Toral R and Serrano M A 2014 *Phys. Rev. E* **90** 042108
- [37] Chen H, Wang S, Shen C, Zhang H and Bianconi G 2020 *Phys. Rev. E* **102** 062311
- [38] Peralta A F, Khalil N and Toral R 2020 *Physica A* **552** 122475
- [39] Artime O, Peralta A F, Toral R, Ramasco J J and San Miguel M 2018 *Phys. Rev. E* **98** 032104
- [40] Peralta A F, Khalil N and Toral R 2020 *J. Stat. Mech.* **024004**
- [41] Abella D, San Miguel M and Ramasco J J 2022 *Sci. Rep.* **12** 19376
- [42] Abella D, San Miguel M and Ramasco J J 2023 *Phys. Rev. E* **107** 024101
- [43] Karsai M, Kivela M, Pan R K, Kaski K, Kertész J, Barabási A L and Saramäki J 2011 *Phys. Rev. E* **83** 025102
- [44] Rybski D, Buldyrev S V, Havlin S, Liljeros F and Makse H A 2009 *Proc. Natl Acad. Sci.* **106** 12640–5
- [45] Zignani M, Esfandyari A, Gaito S and Rossi G P 2016 *Appl. Netw. Sci.* **1** 5
- [46] Artime O, Ramasco J J and San Miguel M 2017 *Sci. Rep.* **7** 41627
- [47] Kumar P, Korkolis E, Benzi R, Denisov D, Niemeijer A, Schall P, Toschi F and Trampert J 2020 *Sci. Rep.* **10** 626
- [48] Erdős P et al 1960 *Publ. Math. Inst. Hung. Acad. Sci.* **5** 17–60
- [49] Wormald N C et al 1999 *Models of Random Regular Graphs (London Mathematical Society)* pp London Mathematical Society 239–98
- [50] Gleeson J P 2013 *Phys. Rev. X* **3** 021004
- [51] Glauber R J 1963 *J. Math. Phys.* **4** 294–307
- [52] Newman M E J, Strogatz S H and Watts D J 2001 *Phys. Rev. E* **64** 026118
- [53] Abella David GitHub repository with the code to solve the Approximate Master Equation (<https://github.com/davidabbu/Aging-in-binary-state-models>)
- [54] Ben-Naim E, Frachebourg L and Krapivsky P L 1996 *Phys. Rev. E* **53** 3078–87
- [55] Haan L and Ferreira A 2006 *Extreme Value Theory: An Introduction* vol 3 (Springer)
- [56] Pournaki A, Olbrich E, Banisch S and Klemm K 2023 Order-disorder transition in the zero-temperature Ising model on random graphs *Phys. Rev. E* **107** 054112
- [57] Stauffer D, Adler J and Aharony A 1994 *J. Phys. A: Math. Gen.* **27** L475–80
- [58] Derrida B 1995 *J. Phys. A: Math. Gen.* **28** 1481–91

- [59] Derrida B, Hakim V and Pasquier V 1995 *Phys. Rev. Lett.* **75** 751–4
- [60] Derrida B 1997 *Phys. Rev. E* **55** 3705–7
- [61] Gunton J 2000 Kinetics of first-order phase transitions *Phase Transitions and Critical Phenomena* vol 8, ed D Cyril and J L Lebowitz (Springer) pp 269–466
- [62] Peralta A F and Toral R 2020 *Phys. Rev. Res.* **2** 043370
- [63] Barabási A L 2009 *Science* **325** 412–3
- [64] Zimmermann M G, Eguíluz V M and San Miguel M 2004 *Phys. Rev. E* **69** 065102
- [65] Vazquez E, Eguíluz V M and Miguel M S 2008 *Phys. Rev. Lett.* **100** 108702